Asymmetry in band widening and quasiparticle lifetimes in $SrVO_3$: Competition between screened exchange and local correlations from combined GW and dynamical mean-field theory GW + DMFT

Jan M. Tomczak,[1] M. Casula,[2] T. Miyake,[3] and S. Biermann[4]

[1]*Institute of Solid State Physics, Vienna University of Technology, A-1040 Vienna, Austria*

[2]*Institut de Minéralogie, de Physique des Matériaux et de Cosmochimie, Université Pierre et Marie Curie, case 115, 4 place Jussieu, 75252, Paris cedex 05, France*

[3]*Nanosystem Research Institute, AIST, Tsukuba 305-8568, Japan*

[4]*Centre de Physique Théorique, Ecole Polytechnique, CNRS-UMR7644, 91128 Palaiseau, France*

(Received 29 December 2013; revised manuscript received 28 August 2014; published 28 October 2014)

The very first dynamical implementation of the combined GW and dynamical mean-field scheme "GW + DMFT" for a real material was achieved recently [Tomczak *et al.*, Europhys. Lett. **100**, 67001 (2012)], and applied to the ternary transition metal oxide $SrVO_3$. Here, we review and extend that work, giving not only a detailed account of full GW + DMFT calculations, but also discussing and testing simplified approximate schemes. We give insights into the nature of exchange and correlation effects: dynamical renormalizations in the Fermi liquid regime of $SrVO_3$ are essentially local, and nonlocal correlations mainly act to screen the Fock exchange term. The latter substantially widens the quasiparticle band structure, while the band narrowing induced by the former is accompanied by a spectral weight transfer to higher energies. Most interestingly, the exchange broadening is more pronounced in the unoccupied part of the spectrum than in the occupied one. In addition, shorter lifetimes for unoccupied states further contribute to making the corrections to the Kohn-Sham band structure asymmetric with respect to the chemical potential. As a result, the GW + DMFT electronic structure of $SrVO_3$ resembles the conventional density functional based dynamical mean-field (DFT + DMFT) description for occupied states but is profoundly modified in the empty part. Our work leads to a reinterpretation of inverse photoemission spectroscopy (IPES) data. Indeed, we assign a prominent peak at about 2.7 eV dominantly to e_g states, rather than to an upper Hubbard band of t_{2g} character. Similar surprises can be expected for other transition metal oxides. This prediction urgently calls for more detailed investigations of conduction band states in correlated materials.

DOI: 10.1103/PhysRevB.90.165138 PACS number(s): 71.27.+a, 71.10.−w, 71.15.Mb

I. INTRODUCTION

Within the last decade, a new research field has developed at the interface of many-body theory and first principles electronic structure calculations. The aim is the construction of materials-specific parameter-free many-body theories that preserve the *ab initio* nature of density functional based methods, but incorporate at the same time a many-body description of Coulomb interactions beyond the independent-electron picture into computational approaches for spectroscopic and finite-temperature properties.

Historically, the first nonperturbative electronic structure techniques for correlated materials evolved from many-body treatments of the multiorbital Hubbard Hamiltonian with realistic parameters. The general strategy of these so-called "LDA++" approaches [1,2] (for reviews see, e.g., Refs. [3–6]) consists in the extraction of the parameters of a many-body Hamiltonian from first-principles calculations and then solving the problem by many-body techniques. In practice, this procedure has met tremendous success in the description of the electronic structure of correlated materials, for a wide range of materials, from transition metals [7,8], their oxides [9–30], sulfides [31,32], or silicides [33,34], to f-electron compounds [35–38]. More recently, iron pnictide compounds (see, e.g., Refs. [39–47]) or spin-orbit materials [48] have come into the focus of many-body electronic structure calculations, emphasizing the need for fully *ab initio* techniques, including a first-principles description of the effective Coulomb interactions. The challenge here is an accurate description of screening of low-energy interactions by high-energy degrees of freedom, the screening of local interactions by nonlocal charge fluctuations [49–51], as well as the capturing of nonlocal exchange and correlation effects [52,53].

Despite the tremendous success of LDA++ schemes, one should be aware of the fact that the ambiguities in the construction of the Hamiltonian are not limited to the many-body part: not even the use of the Kohn-Sham band structure of DFT as a starting Hamiltonian has a direct microscopic justification beyond heuristic arguments. Though renormalization group techniques suggest that in many cases the relevant low-energy effective Hamiltonian can indeed be cast into a generalized (multiorbital) Hubbard form, in practice neither the precise form nor the parameters can be derived directly from the Coulomb Hamiltonian in the continuum. In this sense, the construction of an "LDA++" Hamiltonian amounts to a rather *ad hoc* combination of a Kohn-Sham Hamiltonian and multiorbital Hubbard (and Hund) interaction terms for a subset of "correlated orbitals."

Conceptually, there is moreover a mismatch arising from the fact that the full long-range Coulomb interactions enter the one-particle part of the Hamiltonian (even if only in a mean-field fashion), while in the many-body part, they are replaced by effective local interactions acting only in a low-energy subspace. This has two consequences. The first—well-known one—is related to the double counting correction: correlation effects accounted for in the exchange-correlation potential of DFT have to be subtracted. Yet, a microscopically

motivated definition of this term is, even on a conceptual level, impossible. The second one is more subtle and has only recently started to receive some attention: in fact, the same processes that screen the effective Coulomb interactions are also responsible for renormalizations of the one-body part of the Hamiltonian. This can be understood from an analysis of screening as resulting from coupling of the electrons to bosonic excitations, such as plasmons, particle-hole excitations or more complex many-body processes. The diagonalization of the corresponding electron-boson Hamiltonian results in fermionic quasiparticles ("electronic polarons") corresponding to electrons dressed by their screening bosons, and thus having heavier masses. This mass enhancement corresponds to an effective renormalization of their kinetic energy, and hence of the one-body part of the Hamiltonian. This kind of effect has recently been demonstrated explicitly [54] on the basis of the constrained random phase approximation (cRPA) [55], which allows for an explicit (yet approximate) estimation of dynamical Hubbard interactions in solids. The corresponding one-body renormalizations have been investigated in the framework of dynamical mean-field theory (DMFT) for $SrVO_3$ [56] and $BaFe_2As_2$ [47], and a low-energy effective Hamiltonian comprising these renormalizations has been derived in Ref. [54].

In addition to these effects related to the construction of the LDA++ setup, there are further difficulties arising, when solving the resulting multi-orbital Hubbard Hamiltonian. On the one hand, many approaches, such as those based on dynamical mean-field theory [3,57], neglect *nonlocal* exchange and correlation effects. However, nonlocal self-energy contributions can have a notable influence on the electronic structure of materials, see Refs. [52,53] for the case of the iron pnictides and this paper for $SrVO_3$. On the other hand, while the construction of the one-body part of the Hamiltonian (within DFT) naturally puts the electronic density at the center of the attention, many-body theory is most readily formulated within a Green's function language. This mismatch in language is the final capstone that ensures that matching contributions between the effective one-body Hamiltonian and the many-body terms are truly impossible to identify.

Ideally, the desired specifications of new many-body electronic structure techniques beyond "LDA++" approaches can thus be summarized in three main requirements. (1) The theory should be entirely formulated in the Green's function language, even at the one-body level. (2) The theory should deal directly with the long-range Coulomb interactions, and any effective local "Hubbard-like" interactions should arise only as intermediate auxiliary quantities. (3) At the same time, the theory should retain the nonperturbative character of dynamical mean-field theory, thus avoiding limitations due to a truncation of the perturbation series. This latter point is essential to ensure the scheme to be equally appropriate in the weak, strong and intermediate coupling regimes.

The combination of Hedin's GW approximation—many-body perturbation theory to first order in the screened Coulomb interaction W—and dynamical mean-field theory meets these criteria. Such a scheme was proposed a decade ago [58], based on the construction of the free energy of a solid as a functional of the Green's function G and W.

Only very recently, however, have practical implementations for real materials been achieved [51,59] that go beyond simple static approximation schemes [58,61,62]. The reason was the necessity of dealing with frequency-dependent interactions at the DMFT level, which has remained a major bottleneck until recently. Recent advances in Monte Carlo techniques [63] and the invention of a reliable cumulant-type scheme, the "Bose factor ansatz" [56], have unblocked the situation: two calculations within GW + DMFT taking into account dynamical interactions have been achieved recently, for $SrVO_3$ [59] and for systems of adatoms on surfaces [51]. In this work, we review and extend the former calculations, giving a detailed account of fully dynamical GW + DMFT calculations for $SrVO_3$. The paper is organised as follows. In Sec. II, we give an extensive summary of the concepts of the combined GW + DMFT scheme and discuss aspects of its practical implementation, in particular related to the Bose factor ansatz. Furthermore, we devote an extensive discussion to the question of how to treat multiorbital materials: we propose that for ligand and conduction band shells a perturbative treatment might be sufficient, and show how such a procedure can be combined with the nonperturbative DMFT treatment of the low-energy correlated shells. In Sec. III, we review the electronic structure of our target compound, pointing out problems left open within conventional LDA++ schemes. Section IV presents the results of fully dynamical GW + DMFT calculations, in comparison to GW calculations, LDA + DMFT with static and dynamic interactions, and to simplified combinations of GW and DMFT which allow for a detailed analysis of the importance of the different terms entering the theory. We discuss the implications of our results in Sec. V, before arriving at our conclusions in Sec. VI.

II. THE "GW + DMFT" METHODOLOGY

A. Overview

The starting point of the GW + DMFT scheme is Hedin's GW approximation (GWA) [64], in which the self-energy of a quantum many-body system is obtained from a frequency convolution (or product in time) of the Green's function G with the screened Coulomb interaction $W = \epsilon^{-1}V$. The dielectric function ϵ, which screens the bare Coulomb potential V, is—within a pure GW scheme—obtained from the random phase approximation. The GW + DMFT scheme, as proposed in Ref. [58], combines the first-principles description of screening inherent in GW methods with the nonperturbative nature of DMFT, where local quantities such as the local Green's function are calculated to all orders in the interaction from an effective reference system ("impurity model").[1] In DMFT, one imposes a self-consistency condition for the one-particle Green's function, namely, that its on-site projection equals the impurity Green's function. In GW + DMFT, the self-consistency requirement is generalized to encompass also two-particle quantities, namely, the local projection of the screened interaction is required to equal the impurity

[1]The notion of locality refers to the use of a specific basis set of atom-centered orbitals, such as muffin-tin orbitals, or atom-centered Wannier functions.

screened interaction. This in principle promotes the Hubbard U from an adjustable parameter in DMFT techniques to a self-consistent auxiliary function that incorporates long-range screening effects in an *ab initio* fashion. Indeed, as already alluded to above, not only higher energy degrees of freedom can be downfolded into an effective dynamical interaction, but one can also aim at incorporating nonlocal screening effects into an effective dynamical $\mathcal{U}(\omega)$. The theory is then free of any Hubbard *parameter*, and the interactions are directly determined from the full long-range Coulomb interactions in the continuum.

From a formal point of view, the GW + DMFT method, as introduced in Ref. [58],[2] corresponds to a specific approximation to the correlation part of the free energy of a solid, expressed as a functional of the Green's function G and the screened Coulomb interaction W: the nonlocal part is taken to be the first order term in W, while the local part is calculated from a local impurity model as in (extended) dynamical mean-field theory. This leads to a set of self-consistent equations for the Green's function G, the screened Coulomb interaction W, the self-energy Σ, and the polarization P [65,66]. Specifically, the self-energy is obtained as $\Sigma = \Sigma^{\text{local}} + \Sigma^{\text{nonlocal}}_{GW}$, where the local part Σ_{local} is derived from the impurity model. In practice, however, the calculation of a self-energy for (rather delocalized) s or p orbitals has never been performed within DMFT, and it appears to be more physical to approximate this part also by a GW-like expression. For these reasons, Ref. [59] proposed a practical scheme, in which only the local part of the self-energy of the "correlated" orbitals is calculated from the impurity model and all other local and nonlocal components are approximated by their first order expressions in W.

In the following sections, we first briefly summarize the functional formulation of the GW, DMFT, and GW + DMFT schemes from a general point of view (Sec. II B). The corresponding GW + DMFT equations are summarized in Appendix A. Sections II C and II D are devoted to the "orbital-separated scheme" implemented for $SrVO_3$, defining the equations solved in practice. We then review the dynamic atomic limit approximation for the solution of dynamical impurity models (Sec. II E), while Sec. II F summarizes some technicalities.

B. Unified view on GW, DMFT, and GW + DMFT

Within the Born-Oppenheimer approximation, the electronic many-body states in a solid are determined by the eigenstates of the Coulomb Hamiltonian

$$H = H_{\text{kin}} + H_{\text{pot}} + H_{ee}, \tag{1}$$

where the first two terms denote the kinetic energy part and one-body potential created by the ions, respectively. The last term, $H_{ee} = \sum_{nmn'm'} v_{nmn'm'} a^\dagger_n a^\dagger_m a_{m'} a_{n'}$, with $v_{nmn'm'} = \langle nm|\frac{1}{|r-r'|}|n'm'\rangle$ the matrix elements of the Coulomb interaction in the continuum, denotes the electron-electron interaction.

[2]See also the related scheme of Ref. [60] and the comparison to GW + DMFT in Ref. [50]

Following Almbladh *et al.* [67], the free energy of a solid can be formulated as a functional $\Gamma[G,W]$ of the Green's function G and the screened Coulomb interaction W of the solid. The latter is defined as the correlation function of bosonic excitations corresponding to density fluctuations, that is, in mathematical terms, as the propagator of the Hubbard-Stratonovich field decoupling the Coulomb interaction term. The GW method, dynamical mean-field theory, and the combined GW + DMFT scheme can then be viewed as different approximations to this $\Gamma[G,W]$ functional.

The functional Γ can trivially be split into a Hartree part Γ_H and a many-body correction Ψ, which contains all corrections beyond the Hartree approximation: $\Gamma = \Gamma_H + \Psi$. The Hartree part can be given in the form

$$\begin{aligned}\Gamma_H[G,W] = {} & \text{Tr}\ln G - \text{Tr}\left[\left({G_H}^{-1} - G^{-1}\right)G\right] \\ & - \tfrac{1}{2}\text{Tr}\ln W + \tfrac{1}{2}\text{Tr}\left[\left({V_q}^{-1} - W^{-1}\right)W\right]\end{aligned} \tag{2}$$

with G_H being the Hartree Green's function, and V_q the Fourier transform of the bare Coulomb interaction. The Ψ functional is the sum of all skeleton diagrams that are irreducible with respect to both one-electron propagator and interaction lines. $\Psi[G,W]$ has the following properties:

$$\frac{\delta\Psi}{\delta G} = \Sigma^{\text{xc}}, \quad -2\frac{\delta\Psi}{\delta W} = P. \tag{3}$$

The Ψ functional was first derived in Ref. [67]. A detailed discussion in the context of extended DMFT can be found in Ref. [68], while Refs. [58,65,66] view it from the GW + DMFT point of view.

An elegant derivation (see, e.g., Refs. [51,65,66]) of the Almbladh free energy functional is obtained through a Hubbard Stratonovich decoupling of the interaction term by a bosonic field ϕ, the introduction of Lagrange multipliers Σ and P imposing $\langle cc^\dagger\rangle$ and $\langle\phi\phi\rangle$ to equal externally chosen fermionic and bosonic propagators G and W, and finally, a Legendre transformation to obtain a functional of the latter two quantities.

The GW approximation consists in retaining the first-order term in the screened interaction W only, thus approximating the Ψ functional by

$$\Psi[G,W] = -\tfrac{1}{2}\text{Tr}(GWG). \tag{4}$$

We then trivially find

$$\Sigma^{\text{xc}} = \frac{\delta\Psi}{\delta G} = -GW, \tag{5}$$

$$P = -2\frac{\delta\Psi}{\delta W} = GG. \tag{6}$$

Extended DMFT [69–71], on the other hand, would calculate all local quantities that should be derived from this functional from a local impurity model. One can thus formally write

$$\Psi = \Psi_{\text{imp}}[G^{\text{loc}}, W^{\text{loc}}]. \tag{7}$$

The combined GW + DMFT scheme [58] consists in approximating the Ψ functional as a combination of local and nonlocal parts from GW and extended DMFT, respectively:

$$\Psi = \Psi^{\text{nonloc}}_{GW}[G,W] + \Psi_{\text{imp}}[G^{\text{loc}}, W^{\text{loc}}]. \tag{8}$$

More explicitly, the nonlocal part of the GW + DMFT Ψ functional is given by

$$\Psi^{\text{nonloc}}_{GW}[G,W] = \Psi_{GW}[G,W] - \Psi^{\text{loc}}_{GW}[G,W], \tag{9}$$

while the local part is taken to be an impurity model Ψ functional. Following (extended) DMFT, this on-site part of the functional is generated from a local *quantum impurity problem*. The expression for its free energy functional $\Gamma_{\text{imp}}[G_{\text{imp}},W_{\text{imp}}]$ is analogous to (2) with the Weiss field $\mathcal{G}$ replacing G_H and the Hubbard $\mathcal{U}$ replacing V:

$$\begin{aligned}\Gamma_{\text{imp}}[G_{\text{imp}},W_{\text{imp}}] = {}& \text{Tr}\ln G_{\text{imp}} - \text{Tr}\left[\left(\mathcal{G}^{-1} - G^{-1}_{\text{imp}}\right)G_{\text{imp}}\right] \\ & - \tfrac{1}{2}\text{Tr}\ln W_{\text{imp}} + \tfrac{1}{2}\text{Tr}\left[\left(\mathcal{U}^{-1} - W^{-1}_{\text{imp}}\right)W_{\text{imp}}\right] \\ & + \Psi_{\text{imp}}[G_{\text{imp}},W_{\text{imp}}].\end{aligned} \tag{10}$$

The impurity quantities $G_{\text{imp}}, W_{\text{imp}}$ can thus be calculated from the effective action:

$$\begin{aligned}S = \int d\tau d\tau' \Bigg[& -\sum c^{\dagger}_{L}(\tau)\mathcal{G}^{-1}_{LL'}(\tau-\tau')c_{L'}(\tau') \\ & + \frac{1}{2}\sum : c^{\dagger}_{L_1}(\tau)c_{L_2}(\tau) : \mathcal{U}_{L_1L_2L_3L_4}(\tau-\tau') : \\ & c^{\dagger}_{L_3}(\tau')c_{L_4}(\tau') : \Bigg],\end{aligned} \tag{11}$$

where the sums run over all orbital indices L. In this expression, $c^{\dagger}_{L}$ is a creation operator associated with a localized orbital L, and the double dots denote normal ordering (taking care of Hartree terms). For simplicity, we restrict the discussion to the paramagnetic case and omit any spin indices.

The construction (8) of the Ψ functional is the only *ad hoc* assumption in the GW + DMFT approach. The explicit form of the GW + DMFT equations follows then directly from the functional relations between the free energy, the Green's function, the screened Coulomb interaction etc. Taking derivatives of the functional (8) as in Eq. (3) yields the complete self-energy and polarization operators:

$$\begin{aligned}\Sigma^{\text{xc}}(\mathbf{k},i\omega_n)_{LL'} = {}& \Sigma^{\text{xc}}_{GW}(\mathbf{k},i\omega_n)_{LL'} - \sum_{\mathbf{k}}\Sigma^{\text{xc}}_{GW}(\mathbf{k},i\omega_n)_{LL'} \\ & + \left[\Sigma^{\text{xc}}_{\text{imp}}(i\omega_n)\right]_{LL'},\end{aligned} \tag{12}$$

$$\begin{aligned}P(\mathbf{q},i\nu_n)_{\alpha\beta} = {}& P_{GW}(\mathbf{q},i\nu_n)_{\alpha\beta} - \sum_{\mathbf{q}}P_{GW}(\mathbf{q},i\nu_n)_{\alpha\beta} \\ & + P_{\text{imp}}(i\nu_n)_{\alpha\beta}.\end{aligned} \tag{13}$$

Here, Greek letters indicate a two-particle basis, constructed from the localized (Wannier) basis indexed by L. The *ad hoc* combination of the functional Ψ constructed as a sum of local and nonlocal parts thus leads to a physically attractive result: the off-site part of the self-energy (12) is taken from the GW approximation, whereas the on-site part is calculated to all orders from the dynamical impurity model. This treatment thus goes beyond usual extended DMFT, where the lattice self-energy and polarization are just taken to be their impurity counterparts. The second term in Eq. (12) subtracts the on-site component of the GW self-energy thus avoiding double counting. At self-consistency this term can be rewritten as

$$\sum_{\mathbf{k}}\Sigma^{\text{xc}}_{GW}(\mathbf{k},\tau)_{LL'} = -\sum_{L_1L'_1}W_{\text{imp}}(\tau)_{LL_1L'L'_1}G_{\text{imp}}(\tau)_{L'_1L_1} \tag{14}$$

so that it precisely subtracts the contribution of the GW diagram to the impurity self-energy. Similar considerations apply to the polarization operator.

The general set of GW + DMFT equations to be solved self-consistently is summarized in Appendix. In the following, we discuss a variant, which allows for a physically motivated cheaper treatment of ligand and itinerant empty states.

C. The "orbital-separated" GW + DMFT scheme

In the original GW + DMFT scheme as described in Ref. [58], the Ψ functional is decomposed into nonlocal and local parts, which are then approximated by GW and DMFT, respectively. This means that the local physics of all valence orbitals, including rather itinerant s or p states, would be generated from a self-consistent impurity model. It stands to reason that the self-consistent dynamical $\mathcal{U}$ for those orbitals would in fact come out to be rather small, so that the local dynamical contribution to the self-energy is also small and well described by its first order term in W. In practice, the self-energy for the itinerant states would thus be well described by a perturbative self-energy, that is by the GW self-energy for both, local and nonlocal parts.

In view of these considerations, it seems a waste of computing time to attempt to solve a dynamical impurity models for all valence states, since the same result can be obtained by applying the DMFT construction only to a subset of "correlated" states, and to treat all others entirely by GW. A scheme along these lines was proposed and implemented in Ref. [59].

The equations for the self-energy and polarization are in this case replaced by

$$\begin{aligned}\Sigma^{\text{xc}}(\mathbf{k},i\omega_n)_{LL'} = {}& \Sigma^{\text{xc}}_{GW}(\mathbf{k},i\omega_n)_{LL'} - \sum_{\mathbf{k}}\Sigma^{xc,d}_{GW}(\mathbf{k},i\omega_n)_{LL'} \\ & + \left[\Sigma^{xc,d}_{\text{imp}}(i\omega_n)\right]_{LL'},\end{aligned} \tag{15}$$

$$\begin{aligned}P(\mathbf{q},i\nu_n)_{\alpha\beta} = {}& P_{GW}(\mathbf{q},i\nu_n)_{\alpha\beta} - \sum_{\mathbf{q}}P^{d}_{GW}(\mathbf{q},i\nu_n)_{\alpha\beta} \\ & + P^{d}_{\text{imp}}(i\nu_n)_{\alpha\beta},\end{aligned} \tag{16}$$

where the superscript d denotes the projection onto the low-energy correlated space.

One may be tempted to redefine the Ψ functional as the one of the GW approximation GWG, corrected for its local part by DMFT only within the correlated subspace (denoted here as d), as follows:

$$\begin{aligned}\Psi[G,W] = {}& GWG - G^{\text{loc},d}W^{\text{loc},d}G^{\text{loc},d} \\ & + \Psi_{\text{imp}}[G^{\text{loc},d},W^{\text{loc},d}]\end{aligned} \tag{17}$$

or, alternatively, by keeping the original decomposition into local and nonlocal parts,

$$\Psi[G,W] = \Psi^{\text{nonlocal}} + \Psi^{\text{local}}, \tag{18}$$

but approximating the local one by a combination of GW and DMFT:

$$\Psi^{\rm loc}[G,W] = G^{\rm loc}W^{\rm loc}G^{\rm loc} - G^{{\rm loc},d}W^{{\rm loc},d}G^{{\rm loc},d} + \Psi_{\rm imp}[G^{{\rm loc},d},W^{{\rm loc},d}]. \quad (19)$$

Here, the superscript loc denotes the projection on the local component, and d the projection onto the correlated subspace.

Though appealing at first sight, such combinations cannot be justified without further approximations on a functional basis. This is due to the fact that screening couples the correlated and itinerant subspaces, so that "downfolding" of the interactions to obtain an effective bare interaction within the correlated subspace necessarily involves a decoupling approximation. In the functionals above, this is born out of the difficulty of defining $W^{{\rm loc},d}$, as well as of postulating that $\Psi_{\rm imp}$ is a functional of the Green's function and screened Coulomb interaction of the correlated subspace only.

These considerations have an interesting consequence: indeed, instead of Eqs. (15) and (16), one might have thought of the following equations to define the orbital-separated scheme:

$$\Sigma = \Sigma_{GW} - G^{{\rm loc},d}W^{{\rm loc},d} + \Sigma_{\rm imp}, \quad (20)$$

$$P = GG - G^{{\rm loc},d}G^{{\rm loc},d} + P_{\rm imp}. \quad (21)$$

In the standard (nonorbitally-separated) GW + DMFT scheme (that is, without the d-projections), these equations are equivalent to their counterparts (15) and (16). However, in the orbitally separated scheme, this is no longer the case, since in general

$$\Sigma^{{\rm loc},d} \neq G^{{\rm loc},d}W^{{\rm loc},d}. \quad (22)$$

This is easily seen in the following way, assuming—as in the application below—that the local Green's function is by symmetry diagonal in orbital space: using a symbolic notation for orbitals in the d space and in its complement, denoted as r space, respectively, matrix elements of the d-projected local self-energy read:

$$\Sigma^{{\rm loc},d} = G^{\rm loc}_{dd}W^{\rm loc}_{dddd} + G^{\rm loc}_{rr}W^{\rm loc}_{drrd}. \quad (23)$$

The second term, which stems from the interaction of d-space electrons with r-space ones, can obviously not be derived from a functional $\Psi_{\rm imp}[G^{\rm loc}_{dd},W^{\rm loc}_{dddd}]$.

We note that this difficulty does not arise for the local d-projected polarization, since here

$$P^{{\rm loc},d} = G^{{\rm loc},d}G^{{\rm loc},d} \quad (24)$$

under the assumption of an orbital-diagonal local Green's function.

Summarizing, there are thus two quite intuitive possibilities for the self-consistency in an orbital-separated scheme, namely, (15), (16), (20), and (21), and since there is no functional they can be derived from the choice between them is necessarily *ad hoc*. If one thinks of $\Sigma_{\rm imp}$ as containing only physical processes that live in the local d problem, built with a screened interaction that only knows about screening processes in that subspace, one might be tempted to prefer (20) over (15). Indeed, the term $G^{{\rm loc},d}W^{{\rm loc},d}$ removes only those contributions from the full GW self-energy that find their analog in the impurity self-energy. However, investigating these considerations a bit more deeply, one realises that they crucially rely on the assumption that $\Sigma_{\rm imp}$ be derived from a functional of $G_{\rm imp}$ and $W_{\rm imp}$ only. If, on the contrary, screening processes involving the r-space enter the effective local $\mathcal{U}$ through the fact that the total polarization enters the local d-projected screened interaction,

$$W^{{\rm loc},d} = \left[\sum_{\mathbf{q}}\left(V^{-1}_{\mathbf{q}} - P\right)^{-1}\right]_d, \quad (25)$$

this argument is no longer valid, and (15) might be preferable.

Fortunately, in practice, these conceptual difficulties are not too serious. In fact, numerically, we found the second term in Eq. (23) to be negligible, making the above—*a priori* inequivalent—choices equivalent for all practical purposes. In the following section, we therefore describe the "orbital-separated scheme" used in the present work, where only the local part of the self-energy of the "correlated" orbitals is calculated from the impurity model and all other local and nonlocal components are approximated by their first-order expressions in W.

D. Orbital-separated scheme: the equations

For the reasons discussed above, in the orbital-separated scheme, one deviates from the general prescription Eqs. (12) and (13) for the self-energy and polarization by replacing their local parts by their counterparts generated from an impurity model within the correlated subspace only. We outline in the following the iterative loop obtained at the one-shot GW level but with full self-consistency at the impurity level. We call the correlated subspace d space and its complement the r space. Projections onto these spaces are noted by superscripts. We furthermore assume that we dispose of a Wannier basis that block-diagonalizes the full LDA Hamiltonian, and that the GW self-energy is block-diagonal in the same basis. The Wannier basis can be thought of as obtained from the construction of maximally localized Wannier functions in the d and in the r space separately. The assumption of a vanishing GW self-energy block Σ^{dr} in this basis is an additional approximation [72], which is, however, very accurate, as we have explicitly verified for our target compound $SrVO_3$. We note that the common assumption in GW calculations of a diagonal self-energy in the Kohn-Sham basis is in fact a less justified approximation, and even this is not a severe restriction for $SrVO_3$ [62].

Starting with a guess for the Weiss field and the auxiliary Hubbard $\mathcal{U}$, the impurity model is solved, that is the impurity Green's function $G_{\rm imp}$ and screened Coulomb interaction $W_{\rm imp}$ are obtained. These are matrices in the orbital space of the correlated states only. In order to obtain the full self-energy and polarization, the combined quantities

$$\Sigma = \Sigma_{GW} - \Sigma^{{\rm loc},d}_{GW} + \Sigma_{\rm imp}, \quad (26)$$

$$P = GG - G^{{\rm loc},d}G^{{\rm loc},d} + P_{\rm imp} \quad (27)$$

involve "upfolding" to the full Hilbert space.

Then, the self-consistency equations for the determination of the Weiss mean-field and the auxiliary dynamical $\mathcal{U}$ of the

impurity model require the d projections $G^{\mathrm{loc},d}, W^{\mathrm{loc},d}$ of the local Green's function and screened Coulomb interaction

$$G^{\mathrm{loc}}(\omega) = \sum_k (\omega + \mu - H_0 - \Sigma)^{-1}, \tag{28}$$

$$W^{\mathrm{loc}}(\omega) = \sum_q (V_q - P)^{-1} \tag{29}$$

to equal their impurity model counterparts. In the self-consistency cycle, they are used to update the auxiliary impurity model quantities:

$$\mathcal{G} = (G^{\mathrm{loc},d\,-1} + \Sigma_{\mathrm{imp}})^{-1}, \tag{30}$$

$$\mathcal{U} = (W^{\mathrm{loc},d\,-1} + P_{\mathrm{imp}})^{-1}. \tag{31}$$

The impurity model is solved for these new Weiss field and dynamical $\mathcal{U}$, the resulting impurity Green's function and screened Coulomb interaction are obtained and the cycle is iterated until self-consistency.

In the present work, we resort to a further simplification allowing us to carry out the full self-consistency cycle only for the one-body quantities (Green's function, self-energy, and Weiss field) in the correlated subspace, but to work with fixed dynamical interaction $\mathcal{U}$. This is achieved by approximating P_{imp} in Eq. (27) non-self-consistently by its RPA value $G^{\mathrm{loc},d}G^{\mathrm{loc},d}$ leaving us, see Eq. (27), with $P = GG$ where the LDA Green's function is used for G. Furthermore, we replace Eq. (31) by

$$\mathcal{U} = \left[\sum_q (W^{-1} + P^d)^{-1}\right]_d \tag{32}$$

projected on the d space and its local component. These approximations consist in taking as dynamical impurity $\mathcal{U}$ simply the cRPA estimate for the dynamical Hubbard interaction of the d subspace. This is done by partitioning the RPA polarization into two contributions, P^d and P^r, calculated at the one-shot level from the LDA electronic structure. P^d includes only d-d transitions, while P^r includes all the rest.

For $SrVO_3$, we consider the subset of t_{2g} states as correlated, while oxygen p-, vanadium e_g-, and strontium-d states are considered as r space. The scheme implemented in the present work can then be summarized as follows. (1) Obtain $\mathcal{U}(\omega)$ from a cRPA calculation for a t_{2g} low-energy subspace, that is, as a matrix element:

$$\mathcal{U}(\omega) = \langle \mathrm{t}_{2g}| \frac{V}{1 - V(P - P^{t_{2g}})} |\mathrm{t}_{2g}\rangle. \tag{33}$$

(2) Obtain $\Sigma = GW$ from a one-shot GW calculation, decompose it into the Fock part $\Sigma^x = GV$ and the correlation part $\Sigma^c = GW - GV$. (3) Construct the one-body Hamiltonian

$$H_0 = H_{\mathrm{LDA}} - v^{\mathrm{xc}}_{\mathrm{LDA}} + \Sigma^x, \tag{34}$$

where the LDA exchange-correlation potential has been replaced by the Fock exchange Σ^x. (4) Construct an impurity model in the t_{2g} subspace: start from an educated guess for the Weiss field (in practice, at first iteration we use the LDA local Green's function). (5) Solve the impurity for the Green's function, that is, calculate the expectation value

$$G_{\mathrm{imp}}(\tau) = -\langle \mathcal{T} c(\tau) c^\dagger(0)\rangle_S \tag{35}$$

using the impurity action

$$S = -\int d\tau d\tau' c^\dagger(\tau)\mathcal{G}(\tau - \tau')c(\tau') + \int d\tau H_{\mathrm{inst}} + \int d\tau d\tau' \bar{\mathcal{U}}(\tau - \tau')n(\tau)n(\tau'). \tag{36}$$

Here, H_{inst} denotes the standard Hubbard-Kanamori Hamiltonian for t_{2g} states, parameterized by the intraorbital interaction $U = \mathcal{U}(\omega = 0)$, its interorbital counterpart $U - 2J$, and the interorbital interaction for like-spin electrons $U - 3J$, which is reduced by the Hund's exchange coupling J. The quantity $\bar{\mathcal{U}}(\tau - \tau') = \mathcal{U}(\tau - \tau') - U\delta(\tau - \tau')$ denotes the dynamical interaction without the instantaneous part $U = \mathcal{U}(\omega = 0)$.

(6) From the impurity Green's function, obtain the impurity self-energy via the Dyson equation

$$\Sigma_{\mathrm{imp}} = \mathcal{G}^{-1} - G^{-1}_{\mathrm{imp}}. \tag{37}$$

(7) The full self-energy within the t_{2g} space is obtained by combining the nonlocal GW self-energy, projected onto this subspace, with the impurity self-energy:

$$\Sigma(k, i\omega) = \Sigma_{GW} - \Sigma^{\mathrm{loc},t_{2g}}_{GW} + \Sigma_{\mathrm{imp}}. \tag{38}$$

(8) Calculate the local Green's function within the t_{2g} space using the combined self-energy

$$G^{\mathrm{loc}} = \sum_k [i\omega + \mu - H_0 - \Sigma(k, i\omega)]^{-1} \tag{39}$$

(9) and use this Green's function to update the Weiss field:

$$\mathcal{G} = (G^{\mathrm{loc},t_{2g}\,-1} + \Sigma_{\mathrm{imp}})^{-1}. \tag{40}$$

(10) Go back to the solver step, that is, calculate the impurity Green's function (35) for the impurity model defined by $\mathcal{U}(\omega)$ and the new Weiss field $\mathcal{G}$. (11) Iterate until self-consistency.

E. The Bose factor ansatz

At the heart of the set of GW + DMFT equations is the solution of an impurity model with dynamical interactions. As will be discussed in the results section, the typical energy scale of variation of the latter is the plasma energy, which for transition metal oxides is an order of magnitude larger than the bandwidth. In this limit, the solution of the dynamical impurity model can be greatly simplified. Indeed, the Bose factor ansatz (BFA) within the "dynamic atomic limit approximation" (DALA) introduced in Ref. [56] yields an excellent approximation to the full solution. In this scheme, the Green's function of the dynamical impurity model is obtained from a factorization ansatz:

$$G(\tau) = \left(\frac{G(\tau)}{G_{\mathrm{stat}}(\tau)}\right) G_{\mathrm{stat}}(\tau) \sim \left(\frac{G(\tau)}{G_{\mathrm{stat}}(\tau)}\right)\Big|_{\Delta=0} G_{\mathrm{stat}}(\tau), \tag{41}$$

where G_{stat} is the Green's function for a static impurity model with constant $U = \mathcal{U}(\omega = 0)$, and the first factor is approximated by its value for vanishing bath hybridization Δ [56]. The BFA yields an extremely efficient, yet accurate, way of solving the impurity model, as was checked by benchmarks against direct Monte Carlo calculations in Ref. [56]. It, moreover, allows for a transparent physical interpretation of the arising

spectral properties, since the spectral representation (lowest panel of Fig. 2) of the bosonic renormalization factor that enters Eq. (41),

$$B(\tau) = \left(\frac{G(\tau)}{G_{\rm stat}(\tau)} \right) \Big|_{\Delta=0}, \tag{42}$$

can be interpreted as the density of screening modes [56]. The bosonic factor (42) can be expressed in terms of the frequency-dependent interaction as

$$B(\tau) = \exp\left[-\int_0^\infty \frac{d\omega}{\pi} \frac{\mathrm{Im}\, \mathcal{U}(\omega)}{\omega^2} (K_\tau(\omega) - K_{\tau=0}(\omega)) \right] \tag{43}$$

with the bosonic kernel

$$K_\tau(\omega) = \frac{\exp(-\omega\tau) + \exp(-\omega(\beta-\tau))}{1 - \exp(-\omega\beta)}. \tag{44}$$

F. Technicalities

In the practical calculations for $SrVO_3$, we use the experimental (perfectly cubic perovskite) structure with lattice constant $a = 3.844$ Å. Calculations are performed at inverse temperature $\beta = 10\,\mathrm{eV}^{-1}$ unless otherwise noted. We perform a maximally localized Wannier function construction [75,76] for the t_{2g} part of the Kohn-Sham spectrum within LDA. A one-shot GW calculation is performed within the full valence orbital space and then projected into the t_{2g} space. The GW calculations are performed using a k mesh of $8 \times 8 \times 8$ k points ($4 \times 4 \times 4$ for the ARPES spectra), which is then Wannier interpolated [76] to a dense grid of $27 \times 27 \times 27$ k points for the GW + DMFT calculation.

In one-shot GW calculations (as employed here), the chemical potential is notoriously difficult to place. This is why we have also performed quasiparticle self-consistent (QS)GW [77] calculations (results not shown). There, effects of the self-energy are incorporated into an effective one-particle potential, thus allowing for a precise determination of the chemical potential analogous to DFT techniques. We found k_F to be conserved to its LDA value, as also suggested by angle resolved photoemission spectroscopy results [78].[3] Therefore also in the one-shot GW calculation, we fix the Fermi vector k_F to its LDA value, which thus determines the chemical potential.

In the GW + DMFT, the nonlocal self-energy is fixed at the one-shot level from the initial GW calculation, and the frequency-dependent interaction $\mathcal{U}(\omega)$ at its cRPA value as discussed above. At the DMFT level our calculations are fully self-consistent for all one-particle quantities within the t_{2g} space, determining the self-consistent Weiss field that—together with $\mathcal{U}(\omega)$—defines the auxiliary impurity model, self-consistently solved for fixed nonlocal-GW self-energies. This loop is performed in imaginary time/frequency space at an inverse temperature $\beta = 10\ \mathrm{eV}^{-1}$, allowing at the same time for the chemical potential to adjust self-consistently so as to provide the correct particle number. The resulting Green's functions are analytically continued by means of a maximum entropy algorithm, using the technology of Ref. [56] to access the high-energy features.

III. ELECTRONIC STRUCTURE OF $SrVO_3$

Our target material, $SrVO_3$, has been the subject of intense experimental and theoretical studies (for a review of work until 1998 see Ref. [79]). In this section, we provide a brief summary of our previous knowledge about the electronic properties of this material, in particular concerning photoemission spectroscopy and the corresponding theoretical works.

$SrVO_3$ crystallizes in the cubic perovskite structure: the V^{4+} ions are surrounded by oxygen octahedra, and these octahedra occupy the sites of a simple cubic lattice. The Sr^{2+} cation sits in the center of the cubes. The electron count leaves a single d electron in the V-d states, which is largely responsible for the electronic properties of the compound. The octahedral crystal field splits the V-d states into a lower-lying threefold degenerate t_{2g} manifold, thus filled with one electron per V, and an empty e_g doublet. The compound exhibits a metallic resistivity with a Fermi liquid T^2 behavior up to room-temperature [80] and temperature-independent Pauli paramagnetism without any sign of magnetic ordering [81]. Hall data and NMR measurements confirm the picture of a Fermi liquid with moderate correlations [80,82]. These properties make $SrVO_3$ an ideal model material for studying the effects of electronic Coulomb interactions.

Figure 1 summarizes the Kohn-Sham electronic structure of density functional theory within the local density approximation (LDA): the O-2p states disperse between -2 and -7 eV, separated from the t_{2g} states whose bandwidth extends from -1 to 1.5 eV. While the t_{2g} and e_g bands are well separated at every given k point, the partial density of states (DOS) slightly overlap, and the e_g states display a pronounced peak at 2.3 eV. Finally, peaks stemming from the Sr-d states are located at 6.1 and 7.1 eV. We have superimposed to the LDA DOS the experimental PES and Bremsstrahl-Isochromat spectroscopy (BIS) curves taken from Refs. [73,74]. The comparison reveals the main effects of

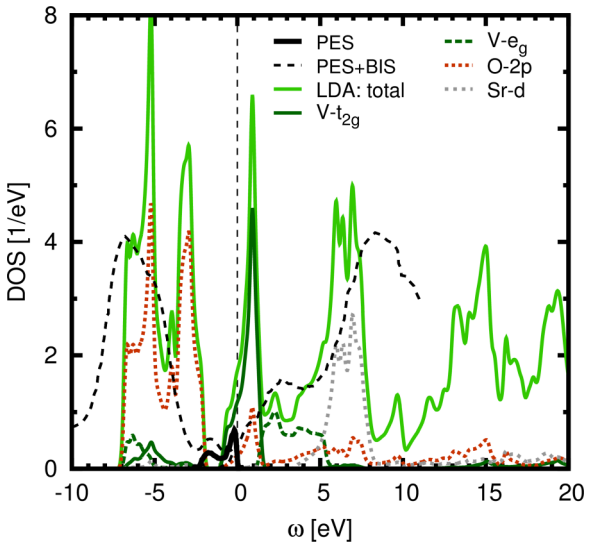

FIG. 1. (Color online) Density of states within LDA in comparison with experimental spectra: PES [73] and PES+BIS [74].

[3] A. Fujimori, private communication.

electronic correlation in this material; as expected on quite general grounds, LDA locates the filled O-2p states at too high and the empty Sr-d manifold at too low energies. The t_{2g} manifold undergoes a strong quasiparticle renormalization with a concomitant shift of spectral weight, both of which are effects beyond the one-particle picture. Photoemission studies [83] early on provided detailed information on the disagreement between the measured spectra and the LDA DOS. In the experimental spectra the t_{2g} spectral weight extends down to binding energies of about -2 eV, i.e., to 1 eV lower than is found in LDA. On the basis of comparison with the Mott insulating compound $YTiO_3$ the observed additional peak between -1.5 and -2 eV was identified as a lower Hubbard band (LHB)—due to the removal process of an electron from an atomic-like localized t_{2g} state—whereas the low-energy spectral weight was attributed to renormalized but coherent band states. A BIS study located an electron addition peak at energies around 2.7 eV [74].

With the advent of dynamical mean-field theory, explicit calculations for spectra for an infinite-dimensional Hubbard model became available [57], supporting the idea of Hubbard bands persisting in the metallic state. The qualitative resemblance of the photoemission spectra with the occupied part of the three-peak structure of the infinite-dimensional one-band Hubbard model suggested $SrVO_3$ to be a prototypical correlated metal, in which the coexistence of quasiparticle states and Hubbard bands as well as their dispersions could be studied. Due to the high symmetry of the crystal structure, and the resulting threefold degeneracy of the t_{2g} bands, it was moreover argued that in a Fermi liquid a purely local self-energy would lead to "pinning" of the value of the fully interacting spectral function at the Fermi level to the one corresponding to the density of states of the one-particle band structure. Any deviation from such "pinning" behavior [84] can thus be taken as a proxy for nonlocal components in the many-body self-energy [74].

A difficulty arose from the extreme surface sensitivity of the photoemission process, as evidenced in Refs. [85–88]. These authors performed systematic photoemission studies at different photon energies, and witnessed a pronounced photon energy dependence of the quasiparticle peak, which they rationalized as a varying surface sensitivity. Measurements at high photon energies (900 eV) [73] indeed found a more developed t_{2g} quasiparticle peak, in agreement with upcoming many-body calculations within dynamical mean-field theory using the LDA density of states (DOS) or the LDA Hamiltonian as input [9,10,14,89]. The increased intensity ratio of the quasiparticle and satellite feature thus suggested nonlocal self-energy effects, neglected in DMFT, to be small. Interestingly, even the surface sensitivity could be modelled within such calculations [90]. Angle-resolved photoemission spectra [91] measuring the Fermi surface of $SrVO_3$ found cylindrical Fermi sheets, in agreement with theory, confirming the picture of a normal Fermi liquid.

Subsequent ARPES work adopted different strategies to increase bulk sensitivity: Laser ARPES [92] studied the very low-energy spectral features, finding a "dip" at the Fermi level or a maximum of the quasiparticle peak slightly below (at around -0.2 eV). This work reopened the question about the role of nonlocal self-energy effects in the very low-energy properties of $SrVO_3$, since it remained unclear whether this feature is a result of the different experimental conditions of the laser ARPES setup (restricted Brillouin zone sampling, matrix elements or other), or whether it reflects the true bulk electronic structure at these very low energies. For a half-filled one-band Hubbard model on a cubic lattice, a similar "dip" effect was indeed found within a cluster dynamical mean-field study [93]. Very recently, a realistic dynamical cluster approximation study [94] confirmed the possibility of nonlocal effects inducing such a depletion at the Fermi level.

Takizawa *et al.* used thin films with atomically flat surfaces prepared *in situ* [95], and were able to observe the band dispersions not only of the coherent band but also of the Hubbard bands. An interesting effect was observed concerning the lower Hubbard band: its intensity is strongly momentum-dependent, with its maximum in regions where also the band states are occupied ($k < k_F$), whereas they fade away for k points corresponding to empty coherent bands [96], in agreement with theoretical modeling within DMFT [95]. Recently, also $SrVO_3$-based heterostructures have been studied experimentally [97] and suggested for electronic device applications [98].

The overall picture which emerges from all these works is that of a correlated metal with a quasiparticle mass enhancement of about 2 [73,74,78,88,95] and a photoemission (Hubbard–)satellite at around -1.6 eV binding energy. This physics is reproduced by dynamical mean-field calculations using the LDA electronic structure as input. The first works [9,10,14,89] used a low-energy model comprising only the t_{2g} manifold, where the local orbitals are constructed from a downfolding procedure that incorporates also the ligand O-2p tails. Different choices of such orbitals were compared [99], demonstrating that as long as the considered energy window is restricted to the t_{2g} bands only, results do not depend on the precise choice of the local orbitals (maximally localized Wannier functions, Nth order muffin-tin orbitals, or projected atomic orbitals).

$SrVO_3$ became the drosophila of combined LDA and DMFT calculations, and new implementations were quite systematically tested on this compound (see, e.g., Refs. [42,99–102]). Apart from the effective t_{2g} model, also Hamiltonians including explicitly V-d and O-2p ligand states in the noninteracting Hamiltonian were used [42,101,102]. It has been argued that the inclusion of ligand states leads to more localized d orbitals, and an *a priori* better justification of the local approximation made by DMFT.

Momentum-resolved spectral functions were calculated from dynamical mean-field theory in Ref. [16], in agreement with the experimental dispersion. They evidenced an additional feature, a "kink" structure at around -0.3 eV binding energy, which was later on rationalized as a generally expected phenomenon in correlated electron materials [103]: of purely electronic origin, kinks appear at the crossover scale at which the low-energy linear (Fermi liquid) behavior of the real part and the quadratic behavior of the imaginary part of the self-energy cease to be valid. In the meanwhile, kink structures observed in other materials, e.g., $LaNiO_3$ [104], were also investigated theoretically and have been consistently reproduced by dynamical mean-field calculations [105]. For $SrVO_3$, the theoretical predictions stimulated an intense search in photoemission spectra. While Ref. [95] still had to conclude

that "the kink is weak and broad, if it exists, but the curvature does indeed change sign at around −0.2 eV, as predicted," the very recent work by Aizaki *et al.* indeed identified such a kink structure at around −0.3 eV [78].

Besides dynamical mean-field theory and extensions, also other techniques of many-body theory were employed to investigate $SrVO_3$. A Gutzwiller study [106] investigated the mass renormalizations, and renormalized densities of states as a function of the Hubbard U. Interestingly, to obtain the experimentally observed mass enhancement a U value beyond 5 eV was found to be necessary in this scheme. Cluster model calculations systematically addressed the spectroscopic properties of $SrVO_3$ and analyzed the necessary ingredients for a minimal model thereof [107–110]. These studies emphasized the strong pd hybridization, which is responsible for the large charge transfer energy $\epsilon_d - \epsilon_p$. Interestingly, an analysis of the orbital character of the different spectral contributions identifies the spectral weight corresponding to the t_{2g} addition process as lying mainly between the Fermi level and about 1 eV, in contradiction with the dynamical mean-field studies which suggest an upper Hubbard band of t_{2g} character at around 2.7 eV, that is at the precise location of the pronounced peak in BIS spectra. The cluster model calculation attributed this latter peak to the electron addition into e_g states [108]. We will come back to this point below.

With the advent of the constrained random phase approximation (cRPA) [55] it became possible to calculate the values of the local Coulomb interactions ("Hubbard U") specifically for the model under consideration. Again, $SrVO_3$ was chosen as a test material to demonstrate the power of the method [111,112], and it was shown that while U values for a full model comprising ligand states as well as V-d states can be as large as 8 eV for the d orbitals, for a t_{2g}-only model the obtained value was quite small: 3.5 eV. The U values used in the above cited LDA + DMFT calculations, on the other hand, varied rather between 4 and 5.5 eV. These values were such as to reproduce the observed mass enhancement, even though the position of the lower Hubbard band (LHB) was generally at slightly too high binding energies, suggesting that these values of U were indeed on the large side. LDA + DMFT calculations with a U value of 3.5 eV, however, do not reproduce the observed mass enhancement, nor result in a clear LHB. This puzzle was solved only recently [56]: it was pointed out that U should be considered as a dynamical quantity rather than a static interaction [55,111]. An LDA + $\mathcal{U}(\omega)$ + DMFT calculation taking not only the *ab initio* value of the static component of $U = 3.5$ eV but also its full frequency dependence into account indeed reproduced the observed mass enhancement as well as the position of the lower Hubbard band [56]. This effect has very recently been confirmed within an analogous study, using a different impurity solver scheme [113].

In the following, we briefly emphasize a few puzzles that remain within the dynamical mean-field description of $SrVO_3$, resulting from the above mentioned works.

Inconsistency between LDA + DMFT and cluster model calculations in the unoccupied part of the spectra. While the assignment of orbital character to the peaks in the spectral function made by the cluster model calculations [108] coincides in the occupied part of the spectra with the results of dynamical mean-field theory [or, to account also for the correct position of the LHB, of LDA + $\mathcal{U}(\omega)$ + DMFT], the position of the upper Hubbard band (UHB) at 2.7 eV found within the LDA + DMFT literature is inconsistent with the cluster model findings.

Interpretation of 2.7 eV BIS feature as an upper Hubbard band inconsistent with ab initio U values. The interpretation of the BIS peak at 2.7 eV as an UHB of t_{2g} character, done in the LDA + DMFT literature, is inconsistent with the static value of U from cRPA. Indeed, from the position of the LHB (∼−1.5 ev) and the static U value (3.5 eV) one would expect an UHB at 2 eV (as found in the LDA + $\mathcal{U}(\omega)$ + DMFT calculation [56]). This leaves the photoemission feature at 2.7 eV unexplained within LDA + DMFT.

Position of O-2p ligand states. LDA + DMFT calculations that also include oxygen ligand orbitals, do not in principle account for corrections to the LDA for these orbitals. Such corrections have been introduced by hand as an arbitrary shift on the O-2p states [42,101]. This means that this position is not known *ab initio* from LDA + DMFT. On the other hand, it is well known that in the related compound $SrTiO_3$, which is isostructural to $SrVO_3$ but of d^0 configuration, the pd gap of Kohn-Sham theory within the LDA is underestimated by 1.3 eV compared to experiment [114].

Position of Sr-4d states. An analogous problem arises when comparing the energetic position of the Sr-4d states in BIS and in Kohn-Sham density functional theory, which underestimates their energy by almost 2 eV. By construction, combined LDA + DMFT schemes do not correct for this error.

Relation between laser ARPES results and nonlocal effects. To the best of our knowledge, it remains open at this stage how to reconcile the laser ARPES experiments (and, in particular, the finding of a dip at the Fermi level) with the high-photon energy PES which display a pronounced peak. The study of nonlocal many-body effects on a very low-energy scale remains thus a challenging task for the future.

The present work addresses the first four issues, leaving the last one for future work. In particular, we review and extend the GW + DMFT calculations of Ref. [59]. Since the publication of Ref. [59], electronic structure calculations for $SrVO_3$ have met renewed interest: besides a study [115] within the GW approximation (including a cumulant correction similar to the above discussed Bose factor ansatz), several groups have embarked into attempts of setting up simplified schemes mimicking the results of GW + DMFT.[4] Interestingly, while different elements of the full calculations are indeed captured in the different schemes, no scheme so far could fully reproduce the low-energy behavior, and the question of designing approximate schemes in a specific low-energy range remains a largely open one. We will therefore also devote an extended paragraph to a systematic comparison of different approximate schemes and a discussion of what they can be expected to provide.

[4]See, e.g., Taranto *et al.* [62] for a study exploring the limits of an implementation with static Hubbard interactions, and—most recently—Sakuma *et al.* [122] who investigated the *ad hoc* combination of an LDA + $\mathcal{U}(\omega)$ + DMFT self-energy with a GW one.

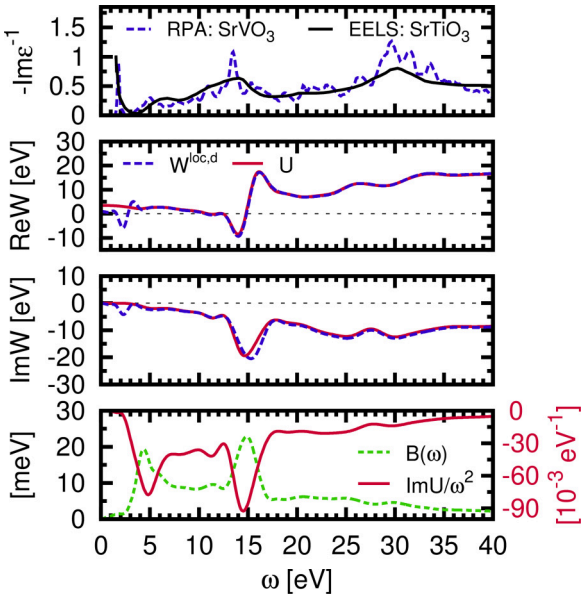

FIG. 2. (Color online) Dynamical screening in $SrVO_3$. From top to bottom: (a) comparison of the inverse dielectric function of $SrVO_3$ within RPA with the experimental EELS spectrum of $SrTiO_3$ [116]. (b)/(c) real/imaginary part of the fully (partially) screened interaction $W^{\mathrm{loc},d}$ ($\mathcal{U}$) in the Wannier basis. (d) Bosonic factor (see text for definition) and density of screening modes $\mathrm{Im}\,\mathcal{U}(\omega)/\omega^2$.

IV. RESULTS

We now turn to the description of the results of GW + DMFT calculations using the formalism outlined above for our target compound, $SrVO_3$. The GW + DMFT calculations will be put into perspective by confronting them to pure GW calculations, as well as to LDA + DMFT calculations both, with static and dynamical interactions. As a prelude, we discuss the dynamical Hubbard interactions obtained for $SrVO_3$ within the cRPA scheme.

A. Dynamical interactions

In Fig. 2, we plot the screened and partially screened Coulomb interactions: W denotes the matrix element of the fully screened interaction in t_{2g} maximally localized Wannier functions and the Hubbard $\mathcal{U}$ is defined in Eq. (33). The physical interpretation of the frequency dependence of the interactions is transparent, if one recalls that the effective bare interaction within a subspace of the original Hilbert space should include screening by the omitted (e.g., higher-energy [55] or nonlocal [117]) degrees of freedom. Indeed, the net result of the rearrangement of the high-energy degrees of freedom as response to a perturbation of the system is an effective reduction of the perturbation strength in the low-energy space. The effective Coulomb interaction in a low-energy effective model for a correlated system is therefore in general an order of magnitude smaller than the matrix element of the bare Coulomb interaction. Nevertheless, the latter is recovered in the limit of high-frequencies of the perturbation, when screening becomes inefficient. The crossover—as a function of frequency—from the low-energy screened regime to the high-frequency bare matrix element of $\frac{e^2}{|\mathbf{r}-\mathbf{r}'|}$ takes place at a characteristic screening (plasma) frequency where the dielectric function exhibits a pole structure.

For $SrVO_3$, the (partially) screened interaction, corresponding to the dynamical Hubbard interaction at vanishing frequency, takes on a value of $U = 3.5$ eV [112] for the t_{2g} orbital-subspace spanned by maximally localized Wannier functions. The corresponding Hund's rule exchange J is 0.6 eV. The bare interaction, the matrix element of the Coulomb interaction within the t_{2g} Wannier orbitals, equals $V = 15$ eV. As seen in Fig. 2, the crossover from the low-energy screened regime to the high-energy tail takes place at about 15 eV. At this energy, a well-defined plasma excitation is observed. Indeed, the upper panel reproduces experimental electron energy loss (EELS) spectra for the related compound $SrTiO_3$ [116]. This material is isostructural to our target compound, and has one electron less (d^0 configuration). The EELS data display a well-defined plasmon excitation at about 15 eV. The experimental spectrum is well-reproduced by the theoretical imaginary part of the inverse dielectric function calculated within the RPA. The reason that, besides higher energy one-particle derived features, also the collective plasmon satellite of d^0 $SrTiO_3$ is well described by our calculation for the nonisoelectronic d^1 $SrVO_3$ resides in the fact that it is not dominated by d-electron contributions. This is evident since the fully and partially screened interaction of the t_{2g} orbitals, W_{t2g} and U_{t2g}, are very similar at these energies. Overall, this validates using the LDA electronic structure for the purpose of calculating the effective interaction $\mathcal{U}(\omega)$ of $SrVO_3$.

The fully screened interaction W furthermore exhibits a weaker feature at low energies ($\sim$2 eV), a "subplasmon," corresponding to a collective charge oscillation of the t_{2g} charge only. This peak is therefore not present when the t_{2g} screening processes are cut out, as is the case in the construction of the effective interaction $\mathcal{U}(\omega)$. As we will see later, this is the energy regime where the local vertex corrections introduced by DMFT modify the GW description of the spectral properties. Features at these energies produced within GW calculations are thus not present any more in the GW + DMFT results (see below).

In the many-body calculation, the frequency-dependent interaction enters the bosonic factor $B(\tau)$ of Eq. (43) in the form of $\mathrm{Im}\,\mathcal{U}(\omega)/\omega^2$. This function can be interpreted as the density of screening modes. It is plotted in the lowest panel of Fig. 2, together with the spectral function of $B(\tau)$ defined in Eq. (42). Interestingly, these functions allow to identify yet another feature, namely a well-defined peak at about 5 eV. We will come back to this point later.

B. GW

Several of the deficiencies of DFT calculations mentioned above can be addressed with Hedin's GW approximation [64], that uses the fully screened interaction W discussed in the previous section. We will in particular address the following two issues. (1) Higher energy states (O-2p, Sr-4d,...). Improvement of these is governed by exchange and correlation effects (beyond DFT) that (i) lie outside the realm of purely local interactions, and (ii) are beyond the (low energy/t_{2g}) orbital subspace. Thus inaccessible to DMFT-based methods, their correction is one pivotal merit that GW contributes to theories

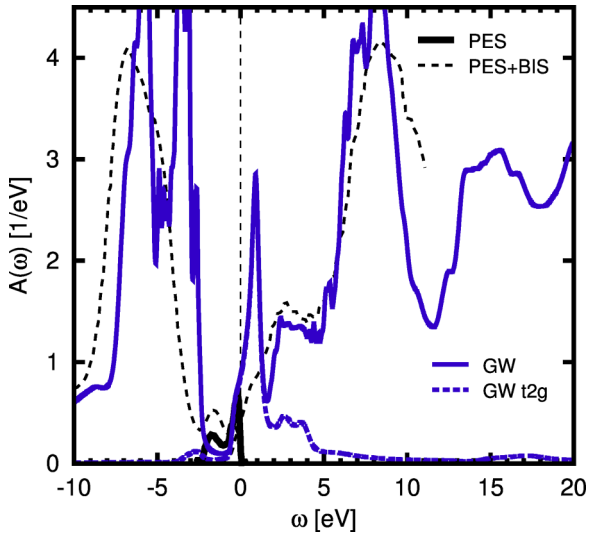

FIG. 3. (Color online) The GW spectral function in comparison to the same experiments as in Fig. 1.

beyond DFT and DFT + DMFT. (2) Many-body effects at low energies. Here we will discuss the impact of many-body renormalization on the t_{2g} spectrum, with particular focus on nonlocal self-energy effects (beyond DFT, and absent in DMFT).

Besides a better description of the electronic structure of $SrVO_3$, our GW calculation also gives useful fundamental insights into the nature of correlation effects in transition metal oxides. We will present evidence that dynamical and nonlocal correlation effects can essentially be separated (this was previously discovered for the iron pnictides and chalcogenides in Ref. [52]). Further we will discuss the spatial extent of correlation effects in real space, putting into perspective corrections to the local picture of DMFT.

1. Correction of higher-energy features

The GW spectral function is shown in Fig. 3. In the unoccupied part of the GW spectrum a substantial improvement over the LDA band-structure result, Fig. 1, is seen: states beyond the t_{2g}s are in excellent agreement with inverse photoemission results. In particular, the hump at around 2–5 eV is very well captured. In contrast to assignments in the DMFT literature, its spectral weight stems largely from the vanadium e_g states within GW, in congruence with cluster based methods [108]. Beyond 5 eV appear the Sr-4d orbitals, again in remarkable accordance with the experimental intensity.

Also the position of occupied states, the O-2p orbitals in the shown energy range, improve to the extent that the experimental satellite at -1.6 eV is no longer obscured by oxygen spectral weight. With respect to the photoemission experiment, however, the binding energy of the O-2p is still too small by at least an electronvolt. A possible remedy to this issue could be to extend the Wannier space to the O-2p and vanadium e_g states and include a local Hubbard interaction on the latter in the GW + DMFT. This would favor a charge transfer into the O-2p orbitals with which the e_g states hybridize most, thus pushing the oxygen states further down. In our GW + DMFT calculations here, we only consider the impact of local Hubbard interactions on the t_{2g} subspace.

2. Low-energy renormalizations

Also shown in Fig. 3 is the t_{2g} contribution to the full spectral function. The t_{2g} bandwidth is reduced by about 25% with respect to LDA, see also the momentum resolved spectra in Figs. 4 and 10. This suggests an overall effective mass $m_{GW}/m_{\mathrm{LDA}} \sim 1.3$. The corresponding spectral weight is transferred to satellites that correspond to the features seen in the fully screened interaction W, see Fig. 2, namely, at $\pm(\sim 2)$ eV as well as the t_{2g} contributions to the plasmon satellite at 17 eV.

To analyze the low-energy renormalizations further, we note that the mass enhancement relative to the LDA band masses is given by the ratio of the magnitudes of the group velocities within LDA, $\frac{d\epsilon_{\mathbf{k}i}}{dk_\alpha} = \langle\Psi_{\mathbf{k}i}|\partial_{k_\alpha} H_{\mathrm{LDA}}(\mathbf{k})|\Psi_{\mathbf{k}i}\rangle_{k=k_F}$, and the GW,

$$\frac{dE_{\mathbf{k}i}}{dk_\alpha} = \left.\frac{\langle\Psi_{\mathbf{k}i}|\partial_{k_\alpha}(H_{\mathrm{LDA}}(\mathbf{k}) + \mathrm{Re}\Sigma_{GW}(\mathbf{k},\omega))|\Psi_{\mathbf{k}i}\rangle}{1 - \langle\Psi_{\mathbf{k}i}|\partial_\omega \mathrm{Re}\Sigma_{GW}(\mathbf{k},\omega)|\Psi_{\mathbf{k}i}\rangle}\right|_{\substack{k=k_F \\ \omega=0}}, \tag{45}$$

evaluated on the Fermi surface. Here, the self-energy is defined with respect to the LDA exchange-correlation

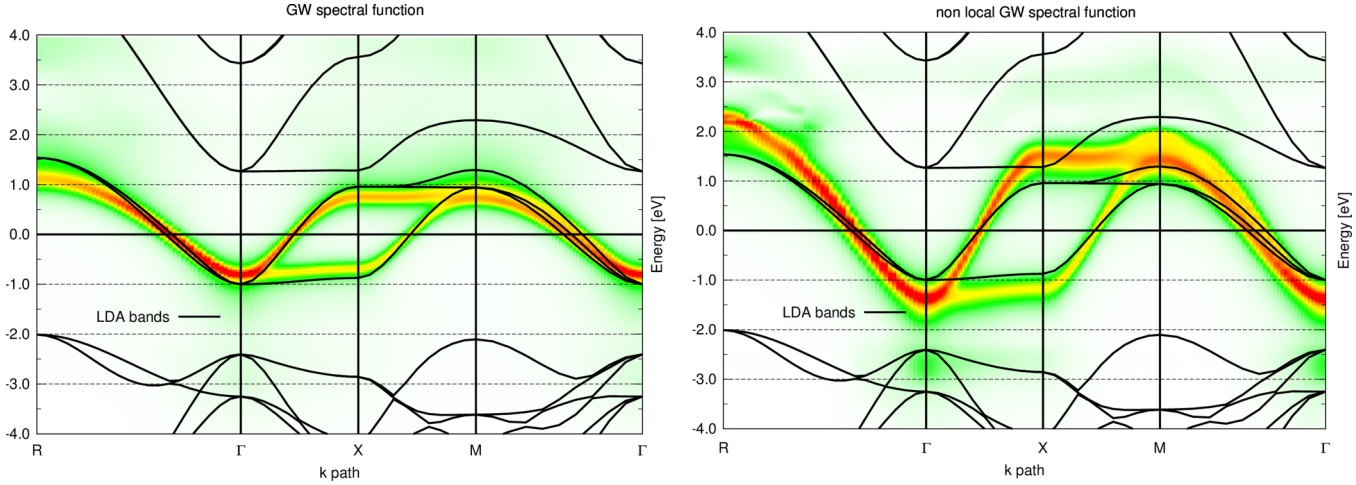

FIG. 4. (Color online) Momentum resolved spectral function (a) within the GW approximation and (b) taking into account only the nonlocal part of the GW self-energy. Superimposed is the LDA band structure.

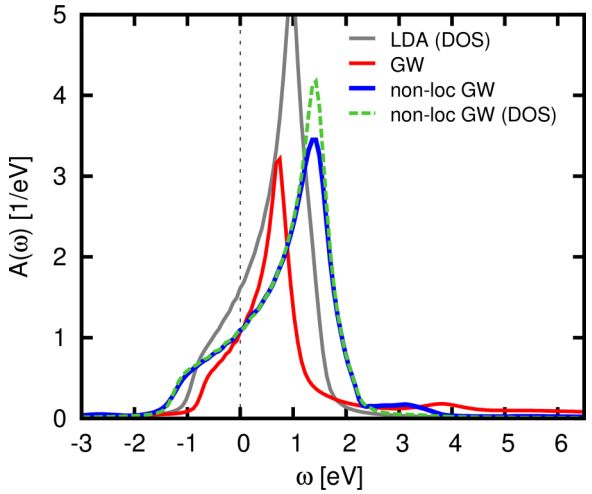

FIG. 5. (Color online) Comparison of the local GW spectral function with the LDA density of states. Also shown is the spectral function Eq. (46) and density of states Eq. (57) of nonlocal-GW. See text for details.

potential: $\Sigma_{GW} = \Sigma^{\rm xc}_{GW} - v^{\rm xc}_{\rm LDA}$. Thus (besides a modified electron density) two ingredients for changes in effective many-body masses can be identified: (a) the *dynamical* part of the self-energy through the quasiparticle weight $Z_{\mathbf{k}} = 1/[1 - \partial_\omega {\rm Re}\Sigma_{GW}(\mathbf{k},\omega)]_{\omega=0}$ and (b) a renormalization via the *nonlocality* of the self-energy, $\partial_{k_\alpha} {\rm Re}\Sigma(\mathbf{k},\omega)$. In DMFT-based approaches, where the self-energy is local by construction, only the first mechanism is present, hence $m_{\rm DMFT}/m_{\rm LDA} = 1/Z_{\rm DMFT}$.[5]

The weight of the t_{2g} quasiparticles in $SrVO_3$ is $Z_{k_F} \sim 0.53$ within the GW approximation. This is virtually the same value that is found for the homogeneous electron gas at the same density, $r_s = 7.26$, when using the same method [64]. The notable inverse quasiparticle weight, $1/Z = 1.9$, in conjunction with the only moderate bandwidth narrowing, $m_{GW}/m_{\rm LDA} = 1.3$, thus advocates a notable enhancement of the group velocity, and thus bandwidth, from nonlocal correlations. We find it instructive to compute the spectral function when only taking into account these nonlocal effects. To this effect, we take out the local part of the GW correlation self-energy and construct $\Sigma^{\rm nonloc}_{GW}(\mathbf{k},\omega) = \Sigma^{\rm xc}_{GW}(\mathbf{k},\omega) - [\Sigma^{\rm xc\ loc}_{GW}(\omega) - \Sigma^{c\ {\rm loc}}(\omega = 0)] - v^{\rm xc}_{\rm LDA}(\mathbf{k})$, where $\Sigma^{c\ {\rm loc}} = \sum_{\mathbf{k}} \Sigma^{c}_{GW}$. The spectral function of this "nonlocal-GW" is shown in Fig. 4(b) for a selected k path, while the local projection (orbital-summed, with m running over the t_{2g} states)

$$A(\omega) = -\frac{1}{\pi} \sum_{k,m=1,2,3} \left[\omega + \mu - \epsilon_{km} - \Sigma^{\rm nonloc}_{GWm}(\mathbf{k},\omega)\right]^{-1} \quad (46)$$

can be seen in Fig. 5. As anticipated, the t_{2g} bandwidth is substantially widened. It becomes 44% larger than the dispersion of the LDA. In particular, we see that this effect is more pronounced in the unoccupied part of the spectrum. DFT being a theory to yield the correct ground state properties (if the exact $v^{\rm xc}$ was known), it seems natural that occupied states are better captured than unoccupied (excited) states (even though of course, the Kohn-Sham spectrum, in principle, has no physical meaning to begin with). This will eventually result in an asymmetric renormalization of the quasiparticle states, with respect to the LDA, as will be discussed below. Interestingly, in $SrVO_3$, a second effect enhances such an asymmetry, namely larger life-time effects in the unoccupied part of the spectrum than in the occupied one. The latter effect can be read off from Fig. 6, middle panel, where the imaginary part of the GW self-energy is plotted.

Also shown in Fig. 5 is the nonlocal-GW density of states, in which all (local and nonlocal) imaginary parts of the GW self-energy are omitted. The presence of nonlocal correlation effects in the GW approximation for $SrVO_3$ can also be evidenced as follows: Indeed, for a purely local self-energy, and in the absence of orbital charge transfers (the t_{2g}-orbitals are locally degenerate), the value of the spectral function at the Fermi level, $A(\omega = 0)$, is "pinned" to its noninteracting (LDA) value [84]. The violation of this pinning condition, see Fig. 5, is thus heralding a nonlocal self-energy. Obviously, the evidenced nonlocal renormalization is also beyond DFT + DMFT approaches, and hence another crucial contribution of the GW to schemes such as GW + DMFT.

Thus the fact that the LDA and GW dispersion are somewhat comparable is owing to the competition and partial cancellation of a bandwidth narrowing through the dynamics

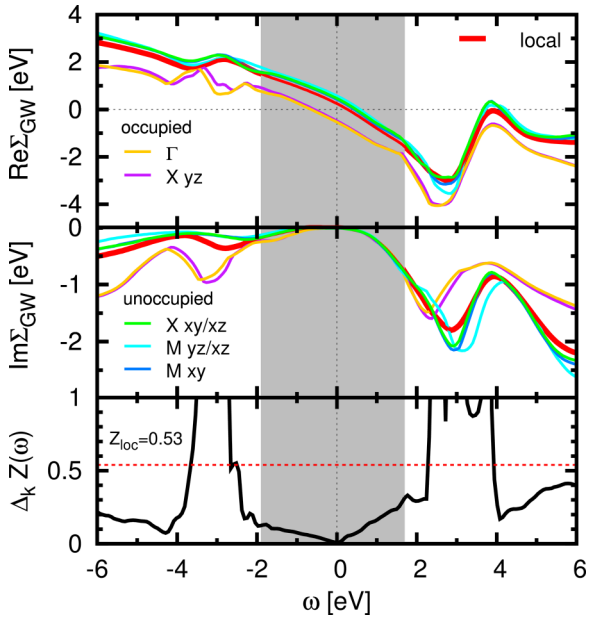

FIG. 6. (Color online) The GW self-energy at several high symmetry points resolved into the three t_{2g} (Wannier) orbitals as a function of frequency. Also shown is the local projection (real parts: top panel, imaginary parts: middle panel). The lower panel displays the standard deviation of the frequency dependent generalization of the quasiparticle weight $Z_{\mathbf{k}}(\omega)$ with respect to its local projection $Z^{\rm loc}(\omega)$ [see Eq. (48)]. The origin of energy corresponds to the Fermi level and the shaded area roughly delimits the Fermi liquid regime within GW.

[5]Of course, the LDA + DMFT self-energy will acquire a trivial momentum dependence when transformed from the local into the Kohn-Sham basis, which is owing to the change in orbital characters for varying momenta.

of the self-energy, and the tendency of nonlocal contributions to delocalize charge carriers. However, the physics underlying these similar dispersions is very different. Indeed, within the GW, almost half of the t_{2g} spectral weight is transferred to collective excitations at higher energies. This phenomenon is absent in effective one-particle theories such as DFT, but a physical reality, see, e.g., the EELS data in the preceding section. However, due to the perturbative nature of GW, and its limitations regarding dynamical local correlations [52], it is not able to reproduce the lower Hubbard satellite seen in photoemission spectroscopy (Fig. 3).

3. Separability of dynamical and nonlocal correlations

Having discussed different ingredients to bandwidth renormalizations, we now examine the nature of correlation effects in more detail. For the case of the iron pnictides and chalcogenides, Tomczak *et al.* [52] found that—within the QSGW approximation—electronic correlation effects in the Fermi liquid regime are *separable* into a dynamical self-energy that is local, and nonlocal contributions that are static. This notion of locality holds when the self-energy is expressed in a local basis, in our case the maximally localized Wannier functions for the t_{2g} subspace. Does this empirical finding extend to the transition metal oxide $SrVO_3$? In the upper panel of Fig. 6, the real part of the GW self-energy of $SrVO_3$ is shown for several high symmetry points in the Brillouin zone as well as the local, i.e., momentum summed, element, as a function of frequency. The offset, $\Sigma_{GW}(\omega = 0)$, is positive for unoccupied orbital characters (xy/xz at the X point, and all t_{2g} orbitals at the M point, cf. Fig. 10), and negative for the occupied orbitals. Thus (un)occupied spectral weight gets pushed (up) down in energy, congruent with the changes in the bandwidth seen in Figs. 5 and 4(b), as well as the reduction of the effective mass m^*/m_{LDA} from the value of the inverse quasiparticle weight $1/Z$ (for a purely local self-energy, $m^*/m_{\mathrm{LDA}} = 1/Z$ holds).

Regarding the frequency dependence, one can see that the self-energy is linear from roughly -2 to $+1.8$ eV, which thus delimits the Fermi liquid regime within the GW approximation. The slope of the self-energy is slightly larger for $\omega > 0$, thus compensating, in part, the static shift that is larger for unoccupied states. Correspondingly, the imaginary part of the self-energy also grows faster with frequency in the unoccupied part, signaling stronger correlations for $\omega > 0$. The important finding here is that in the Fermi liquid regime, the frequency dependence (the linear slope in the real parts) at different momenta is very similar. That is to say that dynamical renormalizations in different regions of the Brillouin zone are comparable. To investigate this more quantitatively, we define

$$Z_{\mathbf{k}}(\omega) = \left[1 - \frac{\partial \mathrm{Re}\Sigma(\mathbf{k},\omega)}{\partial \omega}\right]^{-1} \tag{47}$$

as a generalization of the quasiparticle weight $Z_{k_F}(\omega = 0)$. We further introduce its standard deviation in momentum space [52],

$$\Delta_k Z = \sqrt{\sum_{\mathbf{k}} \mathrm{Tr}|Z_{\mathbf{k}}(\omega) - Z^{\mathrm{loc}}(\omega)|^2}, \tag{48}$$

as defined with respect to the local projection Z^{loc} of Eq. (47), where the trace sums over the Wannier orbitals. Then, $\Delta_k Z$ is a measure for the importance of *dynamical* self-energy effects that are *nonlocal*. As is apparent from Fig. 6, $\Delta_k Z$ virtually vanishes at the Fermi level and is small compared to $Z^{\mathrm{loc}}(\omega = 0) = 0.53$ within the linear regime.[6]

This means that—at least at the GW level[7]—the dynamics of the quasiparticle renormalization in 3D[8] is local, and, conversely, that nonlocal correlation effects are static [52]. As a consequence, the self-energy becomes *separable*; the dynamical part is (almost) purely local, thus providing an *a posteriori* justification for the use of local but dynamic theories such as DMFT. Nonlocal self-energies are static, suggesting that these important effects beyond LDA can be captured by employing generalized (orbital dependent and nonlocal) effective potentials.

This nontrivial finding suggests that for many materials (in and for their Fermi liquid regime) the separation into local and nonlocal self-energies *à la* GW + DMFT simplifies to the extent that nonlocal correlations can be accounted for by a nonlocal yet static potential. This finding may pave the way for physically motivated electronic structure schemes, such as efficient approximations to the full GW + DMFT approach. We will come back to this point in Sec. IV D 2 below.

4. Bandwidth widening by nonlocal self-energy contributions

We now discuss more in detail the widening of the band by nonlocal self-energy contributions, as seen in Fig. 4. To this effect, we note that the separation of the self-energy into a local dynamical and a nonlocal static part [52] can be interpreted as a generalization of the familiar Coulomb-hole-screened exchange (COHSEX) approximation to a full GW treatment. Indeed, in the COHSEX approximation [64] the GW self-energy is given by a static self-energy of the following form:

$$\Sigma(r,r',\omega) = \Sigma_{\mathrm{SEX}}(r,r') + \Sigma_{\mathrm{COH}}(r,r'), \tag{49}$$

[6]It can be shown that the *linear* increase of $\Delta_k Z$ away from the Fermi level stems from the momentum dependence of $\mathcal{O}(\omega^2)$ corrections to $\mathrm{Re}\Sigma(\mathbf{k},\omega)$.

[7]Nonlocal correlation effects beyond the GW picture, stemming, e.g., from fluctuations in the spin-channel, are not included in this discussion. Also, the energy range of validity of the Fermi liquid regime is generally overestimated within the GW approximation, confining the argument to energies lower than suggested by the GW picture. For a discussion beyond GW, see T. Schäfer, A. Toschi, and J. M. Tomczak (unpublished).

[8]Naturally, a nonlocal dynamics is expected in lower dimensional systems, when spin fluctuations (not accounted for in GW) become important, e.g., in the quasi-2D cuprates. In Refs. [49,50], for example, it was found that nonlocal self-energy effects obtained from fluctuations in the charge channel are small within GW + DMFT calculations of an extended Hubbard model, indicating that the leading nonlocal corrections are in the spin channel rather than the charge channel.

where the first term is a screened exchange self-energy built from the static screened Coulomb interaction

$$\Sigma_{\rm SEX}(r,r') = -\sum_{kn}^{occ} \phi_{kn}(r)\phi^*_{kn}(r')W(r,r',\omega=0) \qquad (50)$$

and the second contains the effect of the Coulomb hole:

$$\Sigma_{\rm COH}(r,r') = \tfrac{1}{2}\delta(r-r')[W(r,r',\omega=0) - v(r-r')]. \quad (51)$$

Here, the indices k,n denote Kohn-Sham states of wave vector k, and the sum runs over occupied states only. Interestingly, when separating the COHSEX self-energy into local and nonlocal parts in the many-body sense (that is, with respect to a localized basis set), the nonlocal contribution stems from the screened exchange self-energy only. For a system such as $SrVO_3$, the *local* part of $\Sigma_{\rm SEX}$ is—by symmetry—a scalar in the space of t_{2g} orbitals and can thus be considered an irrelevant constant in that space. The Coulomb hole self-energy, on the other hand, is purely local.

The separation in static nonlocal and dynamical local parts found in the preceding section can therefore be interpreted in the following way. (1) The nonlocal contribution to the self-energy can be mostly attributed to a screened exchange self-energy $\Sigma_{\rm SEX} = GW(\omega=0) - [GW(\omega=0)]_{\rm local}$. (2) The local contribution contains the Coulomb hole effect as well as band renormalizations beyond the COHSEX approximation that stem from the frequency dependence of the local dynamical self-energy.

Therefore, when considering the band structure corresponding to the nonlocal self-energy contribution only, the Coulomb hole part as well as the dynamical correlations are taken out since they are purely local, and the remaining correction can thus largely be interpreted as the screened exchange contribution. The widening of the band as compared to the Kohn-Sham band structure is therefore the familiar broadening by exchange interactions (which, here, are screened, thus leading to substantial but not as large effects as in unscreened Hartree-Fock theory).

The screened exchange self-energy correction to the DFT exchange correlation potential can be written as

$$(\Sigma_{\rm SEX} - v^{\rm xc})(r,r') = -\sum_{k'n'}^{occ} \psi^*_{k'n'}(r)\psi_{k'n'}(r')[W(r,r',\omega=0) - \delta(r-r')\tilde{v}(r)] \qquad (52)$$

with a potential $\tilde{v}(r)$ representing the Kohn-Sham exchange-correlation contribution.

Matrix elements of this quantity in the Kohn-Sham basis read

$$\langle k_0n_0|\Sigma_{\rm SEX} - v^{\rm xc}|k_0n_0\rangle = -\sum_{k'n'}^{occ}\int d^3r\int d^3r'\psi^*_{k'n'}(r)\psi_{k'n'}(r')W(r,r',\omega=0) \times \psi^*_{k_0n_0}(r)\psi_{k_0n_0}(r') + \int d^3r\,\tilde{v}(r)n(r)|\psi_{k_0n_0}(r)|^2. \quad (53)$$

An intuitive inspection of these matrix elements suggests the resulting correction to be small for occupied $|k_0n_0\rangle$ states, but to result in an upward shift for unoccupied states. Indeed, for unoccupied states, the matrix elements $\langle k_0n_0k'n'|W|k_0n_0k'n'\rangle$ are necessarily between product states that mix occupied $|k_0n_0\rangle$ and unoccupied states $|k'n'\rangle$, and thus small compared to $v_{\rm xc}$. This results in the familiar effect of a GW self-energy on the conduction band states in simple semiconductors, correcting the too small Kohn-Sham band gaps.

In the case of the metallic $SrVO_3$ with d^1 filling, the band widening by nonlocal contributions is slightly bigger for the unoccupied part of the spectrum than for the occupied part. As we will see below, this effect will carry through to the GW + DMFT treatment, where the screened exchange band structure becomes renormalized by local dynamical correlations encoded in the DMFT self-energy.

5. The spatial range of correlations

Having established the importance of nonlocal correlation effects, as well as their static nature at low energies, we want to characterize their extent *in real space*. Indeed, there are efforts to extend DMFT calculations from the single impurity setup to a cluster of several sites (or several momenta) even for *ab initio* calculations. For the case of $SrVO_3$, this was first done in Ref. [94] using the dynamical cluster approximation (DCA) method, that partitions the Brillouin zone into momentum patches (two patches, in the cited work) and thus gives momentum resolved information on a coarse grid.

Here, we will rather follow the spirit of cellular DMFT, in which real-space clusters are embedded into the solid, thus allowing for nonlocal correlations of the range of the cluster size. The important question now is how big that cluster has to be in order to exhaust the extent of pertinent nonlocal correlations. For this, we note that self-energy diagrams beyond GW give mainly local contributions [118], and thus our findings based on the GW approximation are expected to have a wide range of validity.[9]

In Fig. 7, we show the magnitudes of the GW self-energy corrections with respect to LDA at the Fermi level ($\omega = 0$) and at energies near the plasmon peak ($\omega = 15$ eV) as a function of the real space distance to a reference vanadium atom.

At the Fermi level, this correction is indeed rather short-ranged; already at the next-nearest (vanadium) neighbor it has decreased by one order of magnitude. This advocates that a $2\times2\times2$ unit-cell cluster (beyond current computational capabilities) might already give meaningful results. For $\omega = 15$ eV, the decrease in magnitude occurs more slowly, suggesting much larger cluster sizes. This does not come as a surprise, since at these energies collective long-ranged (plasmon) excitations are dominant.

C. DMFT

1. DMFT with static interaction

$SrVO_3$ has been used as a benchmark compound for standard LDA + DMFT calculations, both within a low-energy description comprising only the t_{2g} states and including

[9] See, however, the preceding footnote.

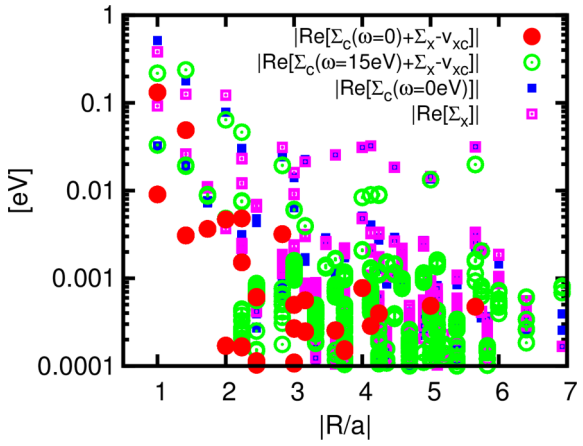

FIG. 7. (Color online) The GW self-energy correction to DFT as a function of real space distance at the Fermi level ($\omega = 0$) and the energy region of the plasmon satellite ($\omega = 15$ eV). The occurrence of several values per distance owes to different orbital orientations at growing numbers of neighbours. Also shown are the absolute values of the ($\omega = 0$) correlation and exchange self-energies of the GW.

the oxygen ligands. It was argued that the static Hubbard interactions have to be at least as large as 4 eV to reproduce the experimentally observed mass enhancement. The local spectral function then displays a three-peak structure as in the correlated metal phase of the half-filled single-band Hubbard model, even though the low filling of one electron in three bands makes the spectra highly asymmetric. The lower Hubbard band, at $U = 4$ eV, is located at slightly too low binding energy (nearly -2eV, instead of the experimentally observed -1.5 eV). At about 2.5 to 2.7 eV, an upper Hubbard band is found. Since this feature coincides in energy with an experimentally observed electron addition peak, the LDA + DMFT literature has thus identified the latter as an upper Hubbard band (see, however, the GW spectrum in Fig. 3 and the discussion below). When using the static component of the Hubbard interaction calculated within cRPA ($\sim$3.5 eV), however, a very weakly correlated metal is obtained, where the lower Hubbard band is barely a shoulder structure and the mass enhancement is much smaller than the experimentally observed one. Figure 8(a) reproduces the local spectral function for U values varying between 3.5 and 4 eV, as calculated in Ref. [99].

2. DMFT with dynamical interaction

The puzzle of the too weak mass renormalizations within LDA + DMFT when the static component of the cRPA U is used was solved when it was realized that taking into account the frequency dependence of the interactions leads to additional mass enhancements [56]. Indeed, the high-energy tail of the dynamical interaction *alone* was shown to be at the origin of a mass enhancement of Z_B^{-1} with $Z_B = 0.7$ [56]. The overall mass enhancement of the calculation with the dynamical cRPA interaction is $m^*/m_{\mathrm{LDA}} \sim 2$, in reasonable agreement with ARPES estimates[78,95]. Since, however, the static component of U is smaller than what was used before in static LDA + DMFT calculations, the position of the lower Hubbard band is shifted towards the Fermi level, correcting the deficiency of LDA + DMFT discussed above. On the unoccupied side of the spectrum, an upper Hubbard band feature appears at about 2 eV, substantially lower than what was discussed within LDA + DMFT, see Fig. 8. Experimentally, such a feature is not clearly resolved. We can thus summarize the effect of dynamical interactions within LDA + $\mathcal{U}(\omega)$ + DMFT calculations by noting that the only notable modification in the electronic structure is the improved description of the lower Hubbard band, compared to experiment, whereas the situation is less clear for the unoccupied part of the spectrum. We will argue below that this scheme is actually as little appropriate for unoccupied states as is the standard static LDA + DMFT.

D. GW + DMFT

1. Full calculations

We now discuss the results of our combined GW + DMFT calculations for the spectral properties of $SrVO_3$. Figures 9(a) and 9(b) displays the local projection of the spectral function, while Fig. 10 shows momentum dependent t_{2g} spectra in comparison with ARPES measurements [78,95]. The global

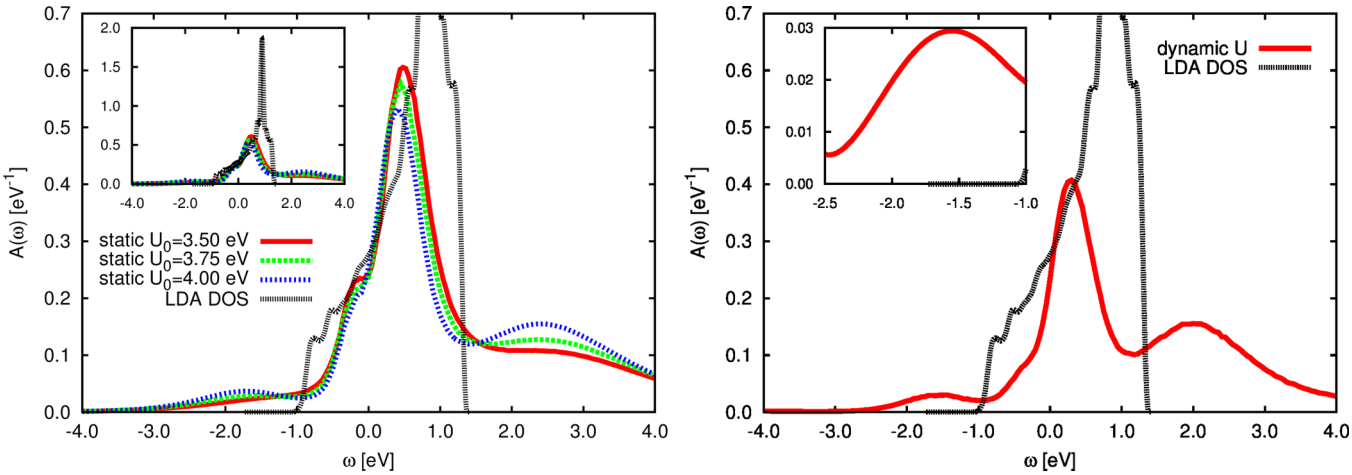

FIG. 8. (Color online) Local spectral function from standard LDA + DMFT with static interactions (left). LDA + DMFT with dynamical interactions (right). Spectral functions are normalized to one, such that the filling corresponding to $SrVO_3$ is 1/6.

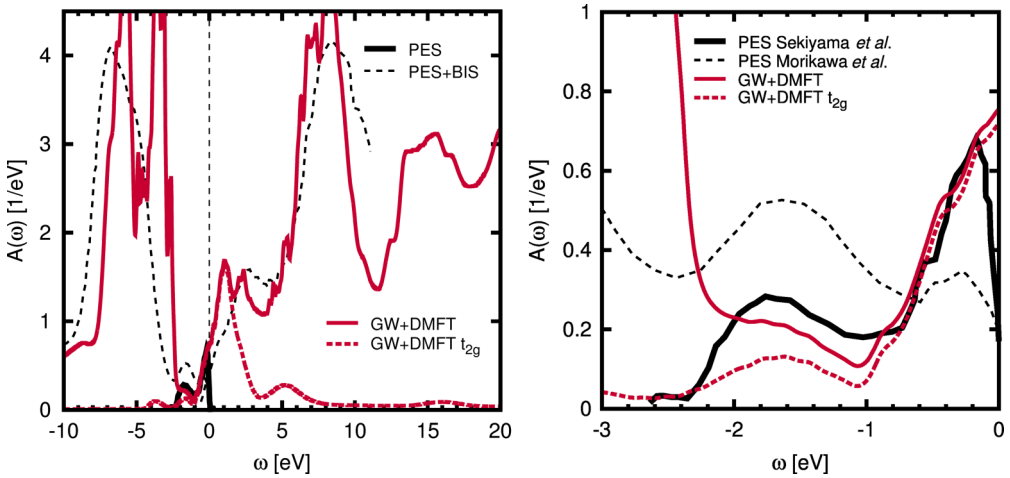

FIG. 9. (Color online) GW + DMFT spectral function for a large (left) and low-energy (right) windows, in comparison to (inverse) photoemission spectra of Refs. [73,74]. Note in particular the appearance of a lower Hubbard at the correct energy in the occupied part of the spectrum, and the fact that the peak at +3 eV in the inverse photoemission spectrum is not derived from a t_{2g} upper Hubbard band, but rather from the e_g orbitals.

view on the spectral function in the full energy range of valence and conduction band states, Fig. 9(a), reveals an overall remarkable agreement with experiments. Indeed, GW + DMFT inherits from the GW calculation the excellent agreement of the Sr-4d states, both, in position and shape, with BIS spectra, and the improved agreement of the O-2p ligand states with photoemission. The low-energy part of the spectrum is dominated by the t_{2g} contribution, which, here, is profoundly modified with respect to pure GW results. A renormalized quasiparticle band disperses around the Fermi level : At the Γ point (see Fig. 10) the peak is located at about −0.5 eV—this reveals (in agreement with ARPES) a strong renormalization of the corresponding Kohn-Sham state which, at this momentum, has an energy of −1 eV. At the X point, the t_{2g} bands are no longer degenerate, and surprisingly weakly renormalized xy/xz states are observed at 0.9 eV, that is, *at the position of the original LDA band states* at this k point. This indicates the extremely weak quasiparticle renormalizations in the unoccupied part of the spectrum, resulting from a strong cancellation effect between exchange widening and narrowing by correlations. The yz band is located at nearly the same energy as at the Γ point, again in agreement with ARPES. At binding energies of −1.6 eV, ARPES witnesses a weakly dispersive Hubbard band, whose intensity varies significantly as a function of momentum [95]. In the GW + DMFT spectral function the Hubbard band—absent in GW—is correctly observed at about −1.6 eV and its k-dependent intensity variation (see Fig. 10) is, indeed, quite strong. Previous LDA + DMFT calculations placed the lower Hubbard band at larger negative energies (see, e.g., Ref. [10]). This is owing to the fact discussed above that when using a static Hubbard interaction, a value of 4–6 eV [10,101], that is larger than the zero frequency limit of the *ab initio* $\mathcal{U}(\omega = 0) = 3.5$ eV [112], is needed to account for the observed transfers of spectral weight. As in DMFT with dynamic $\mathcal{U}$, GW + DMFT yields a good description of the Hubbard band and the spectral weight reduction at the same time, thanks to the additional transfers of spectral weight due to the dynamical screening [54,56,59].

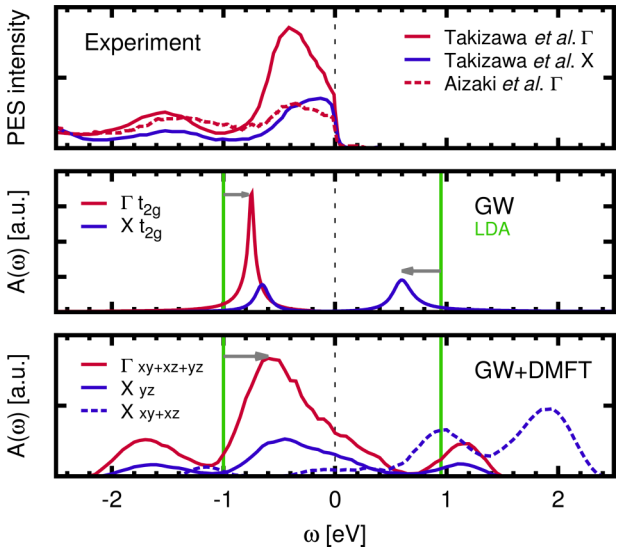

FIG. 10. (Color online) Momentum-resolved spectral function from GW and GW + DMFT in comparison to angle resolved photoemission experiments [78,95]. Also shown is the position of the LDA band at the Γ (lower band edge) and X points. The arrows indicate how these states are renormalized by GW (middle panel) and GW + DMFT (lower panel). Note that the position of the unoccupied LDA band at X coincides with the corresponding quasiparticle peak within GW + DMFT.

At positive energies nonlocal self-energy effects are larger. Interestingly, our k-integrated spectral function [see the dashed line in Fig. 9(a) for the t_{2g} contribution to the total (solid line) spectrum] does not display a clearly separated Hubbard band. The reason is visible from the k-resolved spectra: the upper Hubbard band is located at around 2 eV, as expected from the location of the lower Hubbard band and the fact that their separation is roughly given by the zero-frequency value of U. The peak around 2.7 eV that appears in the inverse photoemission spectrum [74]—commonly interpreted as the upper Hubbard band of t_{2g} character in the DMFT

literature—arises in fact from e_g states located in this energy range. The nonlocal self-energy effects lead, in the unoccupied part of the spectrum, to overlapping features from different k-points and an overall smearing of the total spectral function.

The Bose factor ansatz discussed above does not only provide us with an efficient technique for solving the GW + DMFT equations. It also allows for a transparent physical interpretation of the arising spectral properties. Indeed the spectral representation of the bosonic renormalization factor $B(\tau)$ of Eq. (41) (displayed in the lower panel of Fig. 2) is directly related to the density of screening modes Im $\mathcal{U}(\omega)/\omega^2$ [56]. In this way, we can trace back the GW + DMFT satellite at −4.5 eV to the onset of p-t_{2g} excitations, discussed above for W and U. On the other hand, since the feature below 3 eV in W is absent in U and B, the spurious GW peaks are consistently eliminated. The strong peak at 15 eV is the well-known plasma excitation, seen, e.g., in electron energy loss spectra of $SrTiO_3$ [116].

2. *Test of a simplified scheme: DMFT@nonlocal-GW*

We now turn to the question of how to set up simplified schemes that would still reproduce the results of the full GW + DMFT calculations within the low-energy regime. Besides the methodological interest, this study also allows us to analyze more in detail the dominant effects leading to corrections to the Kohn-Sham band structure.

As can be seen from the methodological section, the DMFT self-consistency condition for the one-body quantities requires the local Green's function to equal

$$G^{\rm loc}(i\omega) = \sum_k \left[i\omega + \mu - H_0(k) - \Sigma^{\rm xc\ nonloc}_{GW}(k,i\omega) - \Sigma_{\rm imp}(i\omega)\right]^{-1} \tag{54}$$

with $H_0 = H_{\rm LDA} - v^{\rm xc}_{\rm LDA}$ from Eq. (34), and $\Sigma^{\rm xc\ nonloc}_{GW}$ is the nonlocal part of the full GW t_{2g} self-energy. The *exchange* contribution to the latter, Σ^{x}_{GW}, is static by construction and can thus be absorbed into an effective Hamiltonian. If also the nonlocal *correlation* self-energy, $\Sigma^c = GW - GV$, were purely static, that is, ω-independent, $\Sigma^{c\ \rm nonloc}_{GW}(k,\omega) = \Sigma^{c\ \rm nonloc}_{GW}(k)$, one could construct an effective quasiparticle Hamiltonian that comprises all nonlocal correlation effects:

$$H^{\rm nl}(k) = H_0(k) + {\rm Re}\Sigma^{\rm xc\ nonloc}_{GW}(k). \tag{55}$$

In Sec. IV B, we have empirically shown (as seen before in Ref. [52] for the iron pnictides) that nonlocal correlations are static within the low-energy Fermi liquid regime. This thus provides a justification for using $H^{\rm nl}$ for the construction of the free (of local correlations) propagator of the DMFT impurity. We will refer to the scheme that uses Eq. (55) as "DMFT@nonlocal-GW", and present here a proof of principle that DMFT@nonlocal-GW yields excellent results for the properties that it was designed for. Of course, the scheme is not expected to give quantitatively accurate results *outside* the quasiparticle energy range. In particular, the dispersion of collective excitations will not be captured. However, their position in the local spectrum which is determined by the structure of the dynamic interaction $\mathcal{U}(\omega)$ is still meaningful as seen below.

For our current material, we can further simplify the approach. Indeed, for the fully degenerate t_{2g} states, the local self-energy is by symmetry a scalar (that is proportional to the 3×3 unit matrix). Equation (54) then reads for each of the three orbital components:

$$G^{\rm loc}(i\omega) - \int d\epsilon D^{\rm eff}(\epsilon) \frac{1}{i\omega + \mu - \epsilon - \Sigma_{\rm imp}(i\omega)}, \tag{56}$$

where we have defined the density of states of the effective nonlocal-GW Hamiltonian $H^{\rm qp}$ as

$$D^{\rm eff}(\epsilon) = -\frac{1}{3\pi}{\rm Im\ Tr}\sum_k [\epsilon - H^{\rm nl}(k) + i0^+]^{-1}. \tag{57}$$

This auxiliary quantity was discussed in the GW section and is plotted in Fig. 5. It contains all information on nonlocal correlations, and is double counting free when combined with the DMFT self-energy. In the current case, where the correlated orbitals are locally degenerate, we can go one step further and include nonlocal life-time effects in this effective density of states:

$$\widetilde{D}^{\rm eff}(\epsilon) = -\frac{1}{3\pi}{\rm Im\ Tr}\sum_k \left[\epsilon - H^{\rm nl}(k) + i{\rm Im}\Sigma^{c\ \rm nonloc}_{GW}(k,\epsilon)\right]^{-1}. \tag{58}$$

Using this density (also shown in Fig. 5) with the cRPA $\mathcal{U}(\omega)$ in the DMFT methodology yields the spectral function that is displayed in Fig. 11(left) along the usual k path. A comparison with Fig. 10 shows a remarkable agreement with the full GW + DMFT dispersion. In Fig. 12 is further shown the local projection of this spectral function in comparison to the full GW + DMFT and the LDA + $\mathcal{U}(\omega)$ + DMFT results. Bearing in mind the different conditions for the analytical continuation necessary to obtain these spectra, the agreement between the DMFT@nonlocal-GW and the full GW + DMFT at low energies is very good: captured are the t_{2g} bandwidth, the position of the lower Hubbard band, the satellite at +4 eV, and even the plasmon at 17 eV. The DMFT@nonlocal-GW approach is thus a promising approach when a full GW + DMFT calculation is too costly.

An obvious advantage that we exploit here is, that it is easier to access the full momentum-resolved spectral function, since an analytical continuation is required only for the local self-energy. From Fig. 11, we observe the asymmetric band renormalization already mentioned before, particularly apparent around the X point. Moreover, we can put it into perspective with yet another effect widely discussed in the literature, namely the appearance of low-energy kink structures around the Fermi energy [78,103,119]. Indeed, a low-energy zoom (see right-hand side of Fig. 11) reveals a change of slope in the quasiparticle dispersion between a very low-energy regime of about $\sim\pm0.1$ eV around the Fermi level and the overall band dispersion. The ratio of the group velocities of the very low-energy dispersion to the LDA one yields a factor of two, roughly corresponding to estimates from effective heat measurements [86]. We add a caveat, however, concerning the precise location in energy of the kink structure: the calculation involves the numerically delicate process of

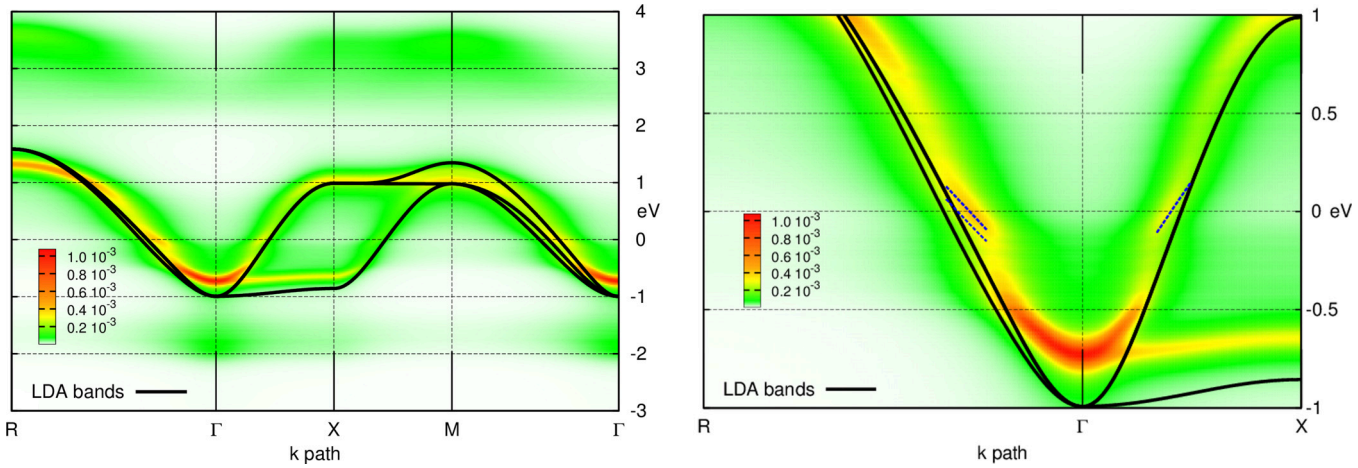

FIG. 11. (Color online) The DMFT@nonlocal-GW approach. The left panel shows the spectral function resolved along the usual momentum path, while the right panel displays a low-energy zoom around the Γ-point. There, the dashed (blue) lines are guides to the eye highlighting the reduced group velocity for energies below the kink in the dispersion (see text for details). The calculation was performed at an inverse temperature $\beta = 10/\text{eV}$. Owing to the large temperature, the Fermi vector k_F is slightly reduced with respect to our LDA (and GW) results.

analytically continuing imaginary frequency data to the real axis, a procedure easily affected with an error bar of 0.1 or 0.2 eV for the position of such subtle structures.

3. *Related approaches: QSGW + DMFT and screened exchange+DMFT*

Interestingly, the prerequisite of having a separable self-energy at the GW level can be relaxed if instead of constructing H^{nl} from a (one-shot) GW calculation, the quasiparticle self-consistency (QS) scheme of Ref. [77] is employed. In the QSGW scheme dynamical self-energies, both local and nonlocal, are incorporated (in a hermitianized form) into an effective one-particle Hamiltonian. In the self-consistency loop, dynamical dependencies are transformed into a generalized orbital- and momentum-dependent static potential. Recently, it was argued [120] that quasiparticle-self-consistency yields the noninteracting Green's function closest to the one of the interacting many-body system. Therewith, also the QSGW + DMFT approach proposed in Ref. [52] is more general than a short-cut requiring a separable self-energy.

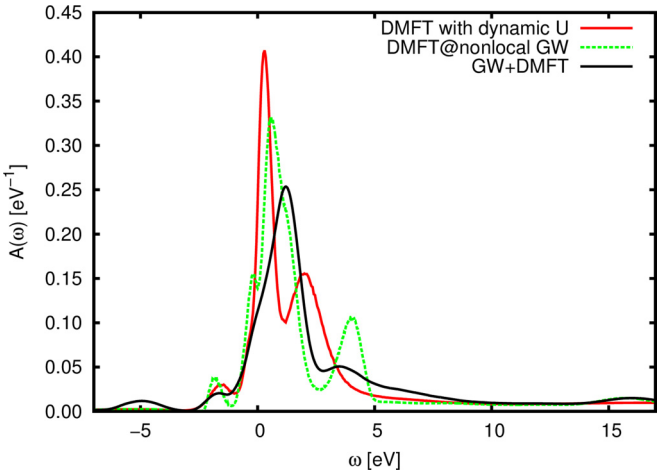

FIG. 12. (Color online) k-summed spectrum of the DMFT@nonlocal-GW approach in comparison with the full GW + DMFT and LDA + $\mathcal{U}(\omega)$ + DMFT. All DMFT calculations were performed at $\beta = 10\,\text{eV}^{-1}$.

A "quasiparticlized" GW (even though at the one-shot level) in combination with DMFT was also studied in Ref. [62], with an application to $SrVO_3$. In this work, however, that scheme was merely used for generating a band structure that was then employed as such as an approximation for a noninteracting Hamiltonian used for DMFT (with static Hubbard interactions). As pointed out in Ref. [52] and immediately obvious from the original GW+DMFT scheme, a consistent combination of QSGW with DMFT must include a correction for avoiding the local GW self-energy to be counted twice. To the best of our knowledge, the form of this correction has not yet explicitly been worked out in the literature. Here, we therefore first define what we mean by QSGW + DMFT before proceeding to a conceptual comparison with the above DMFT@nonlocal-GW scheme.

QSGW proceeds in the following way. First, a GW calculation is performed, and the obtained self-energy is "quasiparticlized" in the following sense: the quasiparticle energies are found (from solving the quasiparticle equation either fully or in a linearized fashion) and the self-energy is evaluated at the corresponding energies E_{kn}. This generates a *static* correction to the initial Hamiltonian [which we will schematically denote as $\Sigma(k,\omega \to H_N^{\text{qp}})$]. Here, the symbolic notation "$\omega \to H_N^{\text{qp}}$" means that the self-energy correction for the state k,n is evaluated at the corresponding quasiparticle energy E_{kn}. The latter is obtained as the pole of the Green's function $[\omega - H_N^{\text{qp}} + V^{\text{xc}} - \Sigma(k,\omega)]^{-1}$.[10] By construction, the corrected Hamiltonian $H_{N+1}^{\text{qp}} = H_N^{\text{qp}} - V_{\text{xc}} + \Sigma(k, H_N^{\text{qp}})$

[10]For simplicity, we do not enter here in a discussion of how to treat off-diagonal self-energy matrix elements and different flavors of choosing the reference energies for those. These issues have been extensively discussed in the literature [123].

then reproduces as eigenvalues the quasiparticle poles of the initial problem $H_N^{\rm qp} - V_{\rm xc} + \Sigma(k,\omega)$. It serves as a starting point for the next iteration, and the process is repeated until convergence is reached. At self-consistency, one can thus think of the obtained Hamiltonian as an optimized one-particle Hamiltonian, motivating its use with DMFT.

In order to combine the QSGW with DMFT, we propose the following scheme: perform a self-consistent QSGW calculation and extract at the last iteration the following quantities: (1) $H^{\rm qp}$ as above, as well as its eigenvalues E_{kn}, (2) $H^{nl} = H^{\rm qp} - \Sigma_{\rm local}(H^{\rm qp})$, where $\Sigma_{\rm local}(\omega) = \sum_k \Sigma(k,\omega)$ is the local self-energy matrix in the localized orbitals. It is quasiparticlized by evaluating it at the eigenvalues E_{kn} of $H^{\rm qp}$. Then, a DMFT calculation (with dynamical $\mathcal{U}$) can be performed on top of H^{nl}, and double counting of the local part is automatically avoided.

We stress that it is essential to substract the local self-energy part before the "quasiparticlization" in the second step. The argument that this term should be a purely constant shift (advanced in Ref. [62]) is in fact incorrect, since the quasiparticlization $\Sigma_{\rm local}(\omega \to H^{\rm qp})$ makes it momentum- and state-dependent. If omitted, the resulting starting Hamiltonian is already renormalized by local dynamical correlations, and application of DMFT leads to a double counting of this renormalization effect, as found in Ref. [62]. Indeed, the band widening induced by the nonlocal part of the self-energy (see discussion above) is then entirely missed, and the band appears too narrow. The crucial issue to realize is that the two operations of quasiparticlization and extraction of the local part (that is, summing over k) do not commute, since the quasiparticlization requires to evaluate the self-energy at a specific energy E_{kn} and thus makes it again k-dependent.

The interesting feature of QSGW is the fact that the final Hamiltonian—through the successive iterations at the quasiparticle level—incorporates corrections that would have been *dynamical* corrections at the one-shot level in an effective static form. In DMFT@nonlocal-GW, on the other hand, we use the empiric observation made at the GW level that the self-energy becomes separable.

Last but not least, we mention yet another simplified scheme that incorporates nonlocal self-energy corrections in a static fashion: between the initial submission and the resubmission of the present work, a combined "screened exchange+DMFT" ("SEx+DMFT") scheme was proposed and implemented [121], which offers a yet numerically cheaper way to incorporate nonlocal effects due to screened exchange.

From a computational point of view, in all three schemes DMFT@nonlocal-GW, QSGW + DMFT and SEx+DMFT, only quantities that *either* depend on frequency *or* momentum enter the DMFT self-consistency, which drastically reduces memory requirements.

4. Further methodological remarks

We now turn to a comparison of the contributions contained in full GW + DMFT, DMFT@nonlocal-GW, and LDA + DMFT with static and dynamical interactions on the basis of the local part of the Matsubara axis self-energies $\Sigma(i\omega)$, plotted in Fig. 13. The most striking feature in the comparison is the small amplitude of the standard LDA + DMFT self-energy. This can be trivially understood from the fact that only the partially screened value of the interaction, the Hubbard U, enters into the description. This scheme does not contain *any* information about the bare interaction—in contrast to all the other schemes, where it is recovered as the high-frequency limit. This information does lead to much higher characteristic energy scales in the schemes beyond LDA + DMFT, with self-energies living on the scale of the plasma energy of ∼15 eV.

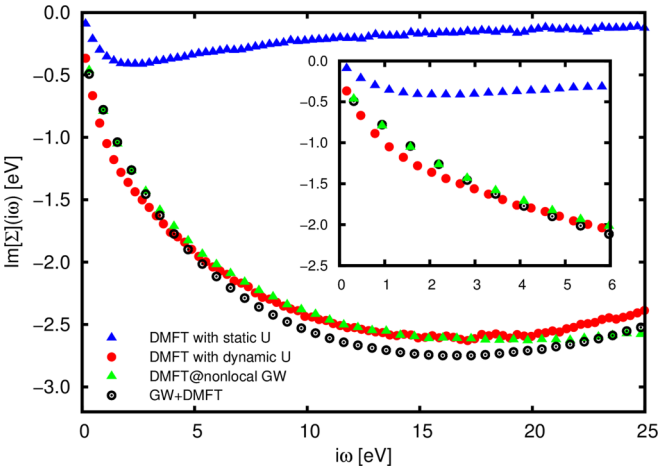

FIG. 13. (Color online) Comparison of local t_{2g} self-energies on the Matsubara axis: usual LDA + DMFT, LDA + DMFT with dynamical interactions, DMFT@nonlocal-GW and local part of full GW + DMFT.

When comparing the shape of the self-energies at low-energies, one can observe that the one for LDA + $\mathcal{U}(\omega)$ + DMFT is slightly steeper, leading to an overestimation of the mass renormalization. The self-consistency loop in the full GW + DMFT scheme leads to a relaxation of the impurity self-energy, and thus less important renormalization effects. The change is in fact quite substantial, leading to different quasiparticle weights corresponding to the different self-energies: while the local Z factor for the fully self-consistent GW + DMFT calculation is nearly 0.7, the LDA + DMFT calculation with dynamical U yields 0.5. A non-self-consistent calculation combining a local LDA + $\mathcal{U}(\omega)$ + DMFT self-energy with a nonlocal-GW self-energy could therefore be expected to underestimate the bandwidth by a factor 0.7/0.5. This may explain why a recent paper for $SrVO_3$ [122] using such a nonselfconsistent "$[\text{LDA} + \mathcal{U}(\omega) + \text{DMFT}]_{\rm local} + [GW]_{\rm nonlocal}$" approach finds a much narrower empty band than our GW + DMFT calculations. This puts strong constraints on the design of simplified schemes: it highlights the importance of having the nonlocal correlations present in the DMFT self-consistency, as done in the DMFT@nonlocal-GW approach discussed above, and also in the QSGW + DMFT scheme [52]. Finally, DMFT@nonlocal-GW and full GW + DMFT agree very well at low energies, as expected from the analysis above, but start to deviate on a scale of several eVs where the nonlocal self-energy correction on the real axis recovers some frequency dependence.

V. SUMMARY

We now come back to the list of physics questions on our target compound, outlined in the introductory section on $SrVO_3$.

Reconciliation of results of DMFT and cluster model calculations in the unoccupied part of the spectra, and consistency with ab initio U values. Our finding of the IPES peak at 2.7 eV being dominantly of e_g character, rather than being an upper Hubbard band of t_{2g} character, coincides with the interpretation of cluster model calculations [108], thus reconciling DMFT with the cluster model literature. Cluster model calculations place an upper Hubbard band of t_{2g} character at about 2 eV, which would be consistent with the static value of $\mathcal{U}(\omega = 0) = 3.5$ eV. The cluster calculations, however, do not have access to the effects of the enhancement of the bare band dispersion by nonlocal exchange. Our GW + DMFT calculations reveal that the latter is in fact the dominant effect, preventing the formation of a clearly separated sharp upper Hubbard band.

The 2.7-eV feature in BIS spectra. Related to the previous point, the photoemission feature at 2.7 eV is *not* an upper Hubbard band, but rather dominated by e_g states. It would be most interesting to perform orbital-resolved inverse photoemission studies to confirm this orbital assignment. A second challenge to inverse photoemission is the question of whether or not the broad feature at lower energies can be resolved into the true lower Hubbard band (at around 2 eV) and the quasiparticle peak dispersing around the Fermi level.

Position of O-2p ligand states. The inclusion of the GW self-energy for the "uncorrelated" states, as explained in the section on the orbital-separated GW + DMFT scheme, introduces corrections on the O-2p ligand states, which are pushed down in energy, improving the agreement with experiment. We note, however, that the size of the correction is not quite large enough, compared to experiment. To some extent, this could have been expected: indeed, we believe feedback effects of the Coulomb interactions on the V-d states (and their hybridization) to be important for determining the O-2p position. However, such effects would only be included if an update of the GW part of the calculation were also performed. This observation thus opens important perspectives for further work.

Position of Sr-4d states. The Sr-4d states are pushed up by the GW self-energy. The total O-2p to Sr-4d energetic distance is enhanced by about 1.25 eV. Comparison with the experimental spectra shows that this correction is excellent in the unoccupied part of the spectrum.

Most importantly, however, we identify a substantial broadening of the unoccupied bandwidth with respect to standard LDA + DMFT calculations. Indeed, the nonlocal part of the GW self-energy, when applied as a correction to the LDA band structure, leads to a widening by more than 40 percent. When local correlations [within DMFT with $\mathcal{U}(\omega)$] are added, the corresponding renormalizations renarrow the unoccupied band roughly such as to recover the original LDA bandwidth. For this reason, while being similar to the LDA + DMFT description for the occupied states, our results suggest an entirely new description for the unoccupied part of the spectrum, calling for a reinvestigation within techniques capturing empty states properties (BIS, IPES, time-resolved ARPES, or similar).

VI. CONCLUSIONS

We have implemented the combined GW + DMFT scheme in a fully dynamical manner, by treating the GW part at the one-shot level, but self-consisting over the DMFT part. Comparisons with pure LDA, pure GW, and LDA + DMFT calculations with static and dynamic interactions allow to assess the importance of the various features of these schemes, such as inclusion of dynamical screening, local and nonlocal self-energy contributions, and self-consistency.

In particular our analysis confirms [52] that at low-energies, the dynamical self-energy contributions of GW or combined GW + DMFT schemes are strongly dominated by the local part, and that the crucial nonlocal corrections are a purely static correction to the LDA exchange correlation potential. This is strongly encouraging in view of the accuracy of DMFT-based schemes for correlated materials, and may allow for shortcuts when going beyond them.

The calculated GW + DMFT spectral functions for $SrVO_3$ are in good agreement with available experimental data for the occupied electronic states. In this part of the spectra, the GW + DMFT scheme only leads to a slight improvement over conventional LDA + DMFT results (provided that in the latter the dynamics of the Hubbard U is included).

Very importantly, however, our GW + DMFT results also suggest, that the *unoccupied* band structure is not well described by many-body calculations based on LDA-derived one-body Hamiltonians. Indeed, broadening by the Fock exchange term is substantial; the appropriate bare band structure for a DMFT-based electronic structure calculation should be wider by about 40% than the corresponding LDA bands, so that the final dispersion *after the many-body calculation* is eventually comparable again to the LDA one.

The mechanism leading to these corrections is quite general: it is based on the simple observation that the exchange-correlation potential of DFT provides a much better approximation to (screened) exchange for occupied electronic states than for empty ones. This, quite generally, suggests that—despite their successes in describing occupied electronic states—*many-body techniques based on LDA Hamiltonians are inappropriate for describing unoccupied states* of correlated transition metal oxides. This is, in particular, true for the combined LDA + DMFT scheme.

These predictions urgently call for experimental studies of correlated oxides by techniques suitable for measuring empty electronic states. Candidates could be bremsstrahl-isochromatography (BIS)/inverse photoemission, time-resolved ARPES, or more indirect probes such as resonant inelastic x-ray scattering (RIXS), optical spectroscopy, or x-ray absorption (XAS).

ACKNOWLEDGMENTS

We acknowledge useful discussions with T. Ayral, A. Georges, K. Held, M. Imada, A.I. Lichtenstein, C. Taranto, A. Toschi, as well as a collaboration with F. Aryasetiawan at the early stage of Ref. [59]. This work was supported by

the French ANR under projects SURMOTT and PNICTIDES, IDRIS/GENCI under projects 091393 and 096493 and the European Research Council through Grant Nos. 306447 and 617196. JMT is grateful for hospitality at CPHT, Ecole Polytechnique, in the framework of a CNRS visiting position.

APPENDIX: THE GW + DMFT EQUATIONS

As discussed in Sec. II B, the GW + DMFT scheme as formulated in Refs. [58,65,66] can be derived as a stationary point (G,W) of the Almbladh free energy functional [67] after approximating the correlation part of this functional by a combination of local and nonlocal terms stemming from DMFT and GW, respectively.

For reference, we here review the equations derived from this construction, leading to an iterative loop which determines $\mathcal{G}$ and $\mathcal{U}$ self-consistently (and, eventually, the full self-energy and polarization operators). (1) The impurity problem (11) is solved, for a given choice of $\mathcal{G}_{LL'}$ and $\mathcal{U}_{\alpha\beta}$: the "impurity" Green's function

$$G_{\rm imp}^{LL'} \equiv -\langle T_\tau c_L(\tau) c_{L'}^+(\tau')\rangle_S \tag{A1}$$

is calculated, together with the impurity self-energy

$$\Sigma_{\rm imp}^{\rm xc} \equiv \delta\Psi_{\rm imp}/\delta G_{\rm imp} = \mathcal{G}^{-1} - G_{\rm imp}^{-1}. \tag{A2}$$

The two-particle correlation function

$$\chi_{L_1L_2L_3L_4} = \left\langle : c_{L_1}^\dagger(\tau) c_{L_2}(\tau) :: c_{L_3}^\dagger(\tau') c_{L_4}(\tau') : \right\rangle_S \tag{A3}$$

must also be evaluated.

(2) The impurity effective interaction is constructed as follows:

$$W_{\rm imp}^{\alpha\beta} = \mathcal{U}_{\alpha\beta} - \sum_{L_1\cdots L_4}\sum_{\gamma\delta} \mathcal{U}_{\alpha\gamma} O_{L_1L_2}^{\gamma} \chi_{L_1L_2L_3L_4} \left[O_{L_3L_4}^{\delta}\right]^* \mathcal{U}_{\delta\beta}, \tag{A4}$$

where $O_{L_1L_2}^{\alpha} \equiv \langle \phi_{L_1}\phi_{L_2}|B^\alpha\rangle$ is the overlap matrix between two-particle states and products of one-particle basis functions.

The polarization operator of the impurity problem is then obtained as

$$P_{\rm imp} \equiv -2\delta\Psi_{\rm imp}/\delta W_{\rm imp} = \mathcal{U}^{-1} - W_{\rm imp}^{-1}, \tag{A5}$$

where all matrix inversions are performed in the two-particle basis B^α (see the discussion in Refs. [65,66]).

(3) From Eqs. (12) and (13), the full $\mathbf{k}$-dependent Green's function $G(\mathbf{k},i\omega_n)$ and effective interaction $W(\mathbf{q},i\nu_n)$ can be constructed. The self-consistency condition is obtained, as in the usual DMFT context, by requiring that the on-site components of these quantities coincide with $G_{\rm imp}$ and $W_{\rm imp}$. In practice, this is done by computing the on-site quantities

$$G^{\rm loc}(i\omega_n) = \sum_{\mathbf{k}} \left[G_H^{-1}(\mathbf{k},i\omega_n) - \Sigma^{\rm xc}(\mathbf{k},i\omega_n)\right]^{-1}, \tag{A6}$$

$$W^{\rm loc}(i\nu_n) = \sum_{\mathbf{q}} \left[V_{\mathbf{q}}^{-1} - P(\mathbf{q},i\nu_n)\right]^{-1}, \tag{A7}$$

and using them to update the Weiss dynamical mean-field $\mathcal{G}$ and the impurity model interaction $\mathcal{U}$ according to

$$\mathcal{G}^{-1} = {G^{\rm loc}}^{-1} + \Sigma_{\rm imp}^{\rm xc}, \tag{A8}$$

$$\mathcal{U}^{-1} = {W^{\rm loc}}^{-1} + P_{\rm imp}. \tag{A9}$$

The set of equations (A1) to (A9) [including (12) and (13)] is iterated until self-consistency.

This in fact means that, conceptually, there are two levels of self-consistency: the one over local quantities, for a given GW calculation, and, eventually, also the update of nonlocal quantities by recalculation of the GW self-energies and polarization. In real materials calculations, this full self-consistency has been only performed once so far, namely in the relatively simple case of a single-orbital system [51]. Here, we restrict ourselves to self-consistency at the DMFT level for a given GW calculation, as discussed in the methodological sections above.

[1] V. I. Anisimov, A. I. Poteryaev, M. A. Korotin, A. O. Anokhin, and G. Kotliar, J. Phys.: Cond. Matter **9**, 7359 (1997).

[2] A. I. Lichtenstein and M. I. Katsnelson, Phys. Rev. B **57**, 6884 (1998).

[3] G. Kotliar and D. Vollhardt, Phys. Today **57**, 53 (2004).

[4] V. I. Anisimov (ed.), *Strong Coulomb Correlations in Electronic Structure Calculations: Beyond the Local Density Approximation* (Gordon and Breach Science Publishers, Amsterdam, The Netherlands, 2000).

[5] S. Biermann, in *Encyclopedia of Materials: Science and Technology*, edited by K. H. J. Buschow, R. W. Cahn, M. C. Flemings, B. Ilschner, E. J. Kramer, S. Mahajan, and P. Veyssiere (Elsevier, Oxford, 2006), pp. 1–9.

[6] K. Held, I. A. Nekrasov, G. Keller, V. Eyert, N. Blümer, A. K. McMahan, R. T. Scalettar, T. Pruschke, V. I. Anisimov, and D. Vollhardt, Physica Status Solidi (b) **243** 2599 (2006); psi-k Newsletter **56** (65) 2003.

[7] A. I. Lichtenstein, M. I. Katsnelson, and G. Kotliar, Phys. Rev. Lett. **87**, 067205 (2001).

[8] S. Biermann, A. Dallmeyer, C. Carbone, W. Eberhardt, C. Pampuch, O. Rader, M. I. Katsnelson, and A. I. Lichtenstein, JETP Lett. **80**, 612 (2004), .

[9] A. Liebsch, Phys. Rev. Lett. **90**, 096401 (2003).

[10] E. Pavarini, S. Biermann, A. Poteryaev, A. I. Lichtenstein, A. Georges, and O. K. Andersen, Phys. Rev. Lett. **92**, 176403 (2004).

[11] K. Held, G. Keller, V. Eyert, D. Vollhardt, and V. I. Anisimov, Phys. Rev. Lett. **86**, 5345 (2001).

[12] G. Keller, K. Held, V. Eyert, D. Vollhardt, and V. I. Anisimov, Phys. Rev. B **70**, 205116 (2004).

[13] A. I. Poteryaev, J. M. Tomczak, S. Biermann, A. Georges, A. I. Lichtenstein, A. N. Rubtsov, T. Saha-Dasgupta, and O. K. Andersen, Phys. Rev. B **76**, 085127 (2007).

[14] I. A. Nekrasov, G. Keller, D. E. Kondakov, A. V. Kozhevnikov, T. Pruschke, K. Held, D. Vollhardt, and V. I. Anisimov, Phys. Rev. B **72**, 155106 (2005).

[15] J. M. Tomczak and S. Biermann, J. Phys.: Condens. Matter **21** 064209 (2009).

[16] I. A. Nekrasov, K. Held, G. Keller, D. E. Kondakov, T. Pruschke, M. Kollar, O. K. Andersen, V. I. Anisimov, and D. Vollhardt, Phys. Rev. B **73**, 155112 (2006).

[17] T. Saha-Dasgupta, A. Lichtenstein, and R. Valentí, Phys. Rev. B **71**, 153108 (2005).

[18] F. Rodolakis, P. Hansmann, J.-P. Rueff, A. Toschi, M. W. Haverkort, G. Sangiovanni, A. Tanaka, T. Saha-Dasgupta, O. K. Andersen, K. Held, M. Sikora, I. Alliot, J.-P. Itié, F. Baudelet, P. Wzietek, P. Metcalf, and M. Marsi, Phys. Rev. Lett. **104**, 047401 (2010).

[19] P. Hansmann, M. W. Haverkort, A. Toschi, G. Sangiovanni, F. Rodolakis, J. P. Rueff, M. Marsi, and K. Held, Phys. Rev. B **85**, 115136 (2012).

[20] X. Wang, M. J. Han, L. de' Medici, H. Park, C. A. Marianetti, and A. J. Millis, Phys. Rev. B **86**, 195136 (2012).

[21] G. Zhang, E. Gorelov, E. Koch, and E. Pavarini, Phys. Rev. B **86**, 184413 (2012).

[22] A. Flesch, G. Zhang, E. Koch, and E. Pavarini, Phys. Rev. B **85**, 035124 (2012).

[23] E. Gorelov, M. Karolak, T. O. Wehling, F. Lechermann, A. I. Lichtenstein, and E. Pavarini, Phys. Rev. Lett. **104**, 226401 (2010).

[24] E. Pavarini and E. Koch, Phys. Rev. Lett. **104**, 086402 (2010).

[25] M. De Raychaudhury, E. Pavarini, and O. K. Andersen, Phys. Rev. Lett. **99**, 126402 (2007).

[26] J. Kuneš, D. M. Korotin, M. A. Korotin, V. I. Anisimov, and P. Werner, Phys. Rev. Lett. **102**, 146402 (2009).

[27] P. Augustinský, V. Křápek, and J. Kuneš, Phys. Rev. Lett. **110**, 267204 (2013).

[28] S. Biermann, A. Poteryaev, A. I. Lichtenstein, and A. Georges, Phys. Rev. Lett. **94**, 026404 (2005).

[29] J. M. Tomczak and S. Biermann, Phys. Status Solidi B **246**, 1996 (2009).

[30] J. M. Tomczak and S. Biermann, Europhys. Lett. **86**, 37004 (2009).

[31] F. Lechermann, S. Biermann, and A. Georges, Phys. Rev. Lett. **94**, 166402 (2005).

[32] F. Lechermann, S. Biermann, and A. Georges, Phys. Rev. B **76**, 085101 (2007).

[33] J. M. Tomczak, K. Haule, and G. Kotliar, Proc. Natl. Acad. Sci. USA **109**, 3243 (2012).

[34] J. M. Tomczak, K. Haule, and G. Kotliar, in *New Materials for Thermoelectric Applications: Theory and Experiment*, NATO Science for Peace and Security Series B: Physics and Biophysics, edited by V. Zlatić and A. Hewson (Springer, Netherlands, 2013) pp. 45–57.

[35] T. Miyake, L. Pourovskii, V. Vildosola, S. Biermann, and A. Georges, J. Phys. Soc. Jpn. Suppl. C **77**, 99 (2008).

[36] J. M. Tomczak, L. V. Pourovskii, L. Vaugier, A. Georges, and S. Biermann, Proc. Natl. Acad. Sci. USA **110**, 904 (2013).

[37] S. Y. Savrasov, G. Kotliar, and E. Abrahams, Nature (London) **410**, 793 (2001).

[38] K. Held, A. K. McMahan, and R. T. Scalettar, Phys. Rev. Lett. **87**, 276404 (2001).

[39] K. Haule, J. H. Shim, and G. Kotliar, Phys. Rev. Lett. **100**, 226402 (2008).

[40] S. L. Skornyakov, A. V. Efremov, N. A. Skorikov, M. A. Korotin, Y. A. Izyumov, V. I. Anisimov, A. V. Kozhevnikov, and D. Vollhardt, Phys. Rev. B **80**, 092501 (2009).

[41] V. I. Anisimov, D. M. Korotin, M. A. Korotin, A. V. Kozhevnikov, J. Kunes, A. O. Shorikov, S. L. Skornyakov, and S. V. Streltsov, J. Phys.: Condens. Matter **21**, 075602 (2009).

[42] M. Aichhorn, L. Pourovskii, V. Vildosola, M. Ferrero, O. Parcollet, T. Miyake, A. Georges, and S. Biermann, Phys. Rev. B **80**, 085101 (2009).

[43] M. Aichhorn, S. Biermann, T. Miyake, A. Georges, and M. Imada, Phys. Rev. B **82**, 064504 (2010).

[44] P. Hansmann, R. Arita, A. Toschi, S. Sakai, G. Sangiovanni, and K. Held, Phys. Rev. Lett. **104**, 197002 (2010).

[45] H. Lee, Y.-Z. Zhang, H. O. Jeschke, and R. Valentí, Phys. Rev. B **81**, 220506 (2010).

[46] J. Ferber, K. Foyevtsova, R. Valentí, and H. O. Jeschke, Phys. Rev. B **85**, 094505 (2012).

[47] P. Werner, M. Casula, T. Miyake, F. Aryasetiawan, A. J. Millis, and S. Biermann, Nat. Phys. **8**, 331 (2012).

[48] C. Martins, M. Aichhorn, L. Vaugier, and S. Biermann, Phys. Rev. Lett. **107**, 266404 (2011).

[49] T. Ayral, P. Werner, and S. Biermann, Phys. Rev. Lett. **109**, 226401 (2012).

[50] T. Ayral, S. Biermann, and P. Werner, Phys. Rev. B **87**, 125149 (2013).

[51] P. Hansmann, T. Ayral, L. Vaugier, P. Werner, and S. Biermann, Phys. Rev. Lett. **110**, 166401 (2013).

[52] J. M. Tomczak, M. van Schilfgaarde, and G. Kotliar, Phys. Rev. Lett. **109**, 237010 (2012).

[53] V. Brouet, P.-H. Lin, Y. Texier, J. Bobroff, A. Taleb-Ibrahimi, P. Le Fèvre, F. Bertran, M. Casula, P. Werner, S. Biermann, F. Rullier-Albenque, A. Forget, and D. Colson, Phys. Rev. Lett. **110**, 167002 (2013).

[54] M. Casula, P. Werner, L. Vaugier, F. Aryasetiawan, T. Miyake, A. J. Millis, and S. Biermann, Phys. Rev. Lett. **109**, 126408 (2012).

[55] F. Aryasetiawan, M. Imada, A. Georges, G. Kotliar, S. Biermann, and A. I. Lichtenstein, Phys. Rev. B **70**, 195104 (2004).

[56] M. Casula, A. Rubtsov, and S. Biermann, Phys. Rev. B **85**, 035115 (2012).

[57] A. Georges, G. Kotliar, W. Krauth, and M. J. Rozenberg, Rev. Mod. Phys. **68**, 13 (1996).

[58] S. Biermann, F. Aryasetiawan, and A. Georges, Phys. Rev. Lett. **90**, 086402 (2003).

[59] J. M. Tomczak, M. Casula, T. Miyake, F. Aryasetiawan, and S. Biermann, Europhys. Lett. **100**, 67001 (2012).

[60] P. Sun and G. Kotliar, Phys. Rev. B **66**, 085120 (2002).

[61] K. Karlsson, J. Phys.: Condens. Matter **17**, 7573 (2005).

[62] C. Taranto, M. Kaltak, N. Parragh, G. Sangiovanni, G. Kresse, A. Toschi, and K. Held, Phys. Rev. B **88**, 165119 (2013).

[63] P. Werner and A. J. Millis, Phys. Rev. Lett. **104**, 146401 (2010).

[64] L. Hedin, Phys. Rev. **139**, A796 (1965).

[65] S. Biermann, F. Aryasetiawan, and A. Georges, *Physics of Spin in Solids: Materials, Methods, and Applications* (Kluwer Academic, Dordrecht, 2004), pp. 43–65.

[66] F. Aryasetiawan, S. Biermann, and A. Georges, *Proceedings of the Conference on Coincidence Studies of Surfaces, Thin Films and Nanostructures, Ringberg castle, September 2003*, edited by J. Berakdar and J. Kirschner (Wiley-VCH Verlag GmbH & Co. KGaA, Weinheim, 2004).

[67] C.-O. Almbladh, U. V. Barth, and R. V. Leeuwen, Int. J. Mod. Phys. B **13**, 535 (1999).

[68] R. Chitra and G. Kotliar, Phys. Rev. B **63**, 115110 (2001).
[69] H. Kajueter, Ph.D. thesis, Rutgers University, 1996.
[70] Q. Si and J. L. Smith, Phys. Rev. Lett. **77**, 3391 (1996).
[71] A. M. Sengupta and A. Georges, Phys. Rev. B **52**, 10295 (1995).
[72] F. Aryasetiawan, J. M. Tomczak, T. Miyake, and R. Sakuma, Phys. Rev. Lett. **102**, 176402 (2009).
[73] A. Sekiyama, H. Fujiwara, S. Imada, S. Suga, H. Eisaki, S. I. Uchida, K. Takegahara, H. Harima, Y. Saitoh, I. A. Nekrasov, G. Keller, D. E. Kondakov, A. V. Kozhevnikov, T. Pruschke, K. Held, D. Vollhardt, and V. I. Anisimov, Phys. Rev. Lett. **93**, 156402 (2004).
[74] K. Morikawa, T. Mizokawa, K. Kobayashi, A. Fujimori, H. Eisaki, S. Uchida, F. Iga, and Y. Nishihara, Phys. Rev. B **52**, 13711 (1995).
[75] I. Souza, N. Marzari, and D. Vanderbilt, Phys. Rev. B **65**, 035109 (2001).
[76] N. Marzari, A. A. Mostofi, J. R. Yates, I. Souza, and D. Vanderbilt, Rev. Mod. Phys. **84**, 1419 (2012).
[77] S. V. Faleev, M. van Schilfgaarde, and T. Kotani, Phys. Rev. Lett. **93**, 126406 (2004).
[78] S. Aizaki, T. Yoshida, K. Yoshimatsu, M. Takizawa, M. Minohara, S. Ideta, A. Fujimori, K. Gupta, P. Mahadevan, K. Horiba, H. Kumigashira, and M. Oshima, Phys. Rev. Lett. **109**, 056401 (2012).
[79] M. Imada, A. Fujimori, and Y. Tokura, Rev. Mod. Phys. **70**, 1039 (1998).
[80] M. Onoda, H. Ohta, and H. Nagasawa, Solid State Commun. **79**, 281 (1991).
[81] I. Inoue, H. Makino, I. Hase, M. Ishikawa, N. Hussey, and M. Rozenberg, Physica B: Condens. Matter **237-238**, 61 (1997).
[82] H. Eisaki, Ph.D. thesis, Tokyo University, 1991.
[83] A. Fujimori, I. Hase, H. Namatame, Y. Fujishima, Y. Tokura, H. Eisaki, S. Uchida, K. Takegahara, and F. M. F. de Groot, Phys. Rev. Lett. **69**, 1796 (1992).
[84] E. Müller-Hartmann, Zeitschrift für Physik B Condensed Matter **76**, 211 (1989).
[85] I. Inoue, Ph.D. thesis, Tokyo University, 1998.
[86] I. H. Inoue, O. Goto, H. Makino, N. E. Hussey, and M. Ishikawa, Phys. Rev. B **58**, 4372 (1998).
[87] K. Maiti, D. D. Sarma, M. J. Rozenberg, I. H. Inoue, H. Makino, O. Goto, M. Pedio, and R. Cimino, Europhys. Lett. **55**, 246 (2001).
[88] K. Maiti, U. Manju, S. Ray, P. Mahadevan, I. H. Inoue, C. Carbone, and D. D. Sarma, Phys. Rev. B **73**, 052508 (2006).
[89] E. Pavarini, A. Yamasaki, J. Nuss, and O. K. Andersen, New J. Phys. **7**, 188 (2005).
[90] H. Ishida, D. Wortmann, and A. Liebsch, Phys. Rev. B **73**, 245421 (2006).
[91] T. Yoshida, K. Tanaka, H. Yagi, A. Ino, H. Eisaki, A. Fujimori, and Z.-X. Shen, Phys. Rev. Lett. **95**, 146404 (2005).
[92] R. Eguchi, T. Kiss, S. Tsuda, T. Shimojima, T. Mizokami, T. Yokoya, A. Chainani, S. Shin, I. H. Inoue, T. Togashi, S. Watanabe, C. Q. Zhang, C. T. Chen, M. Arita, K. Shimada, H. Namatame, and M. Taniguchi, Phys. Rev. Lett. **96**, 076402 (2006).
[93] Y. Z. Zhang and M. Imada, Phys. Rev. B **76**, 045108 (2007).
[94] H. Lee, K. Foyevtsova, J. Ferber, M. Aichhorn, H. O. Jeschke, and R. Valentí, Phys. Rev. B **85**, 165103 (2012).
[95] M. Takizawa, M. Minohara, H. Kumigashira, D. Toyota, M. Oshima, H. Wadati, T. Yoshida, A. Fujimori, M. Lippmaa, M. Kawasaki, H. Koinuma, G. Sordi, and M. Rozenberg, Phys. Rev. B **80**, 235104 (2009).
[96] T. Yoshida, M. Hashimoto, T. Takizawa, A. Fujimori, M. Kubota, K. Ono, and H. Eisaki, Phys. Rev. B **82**, 085119 (2010).
[97] K. Yoshimatsu, T. Okabe, H. Kumigashira, S. Okamoto, S. Aizaki, A. Fujimori, and M. Oshima, Phys. Rev. Lett. **104**, 147601 (2010).
[98] Z. Zhong, M. Wallerberger, J. M. Tomczak, C. Taranto, N. Parragh, A. Toschi, G. Sangiovanni, and K. Held, arXiv:1312.5989 [cond-mat.str-el].
[99] F. Lechermann, A. Georges, A. Poteryaev, S. Biermann, M. Posternak, A. Yamasaki, and O. K. Andersen, Phys. Rev. B **74**, 125120 (2006).
[100] G. Trimarchi, I. Leonov, N. Binggeli, D. Korotin, and V. I. Anisimov, Journal of Physics: Condens. Matter **20**, 135227 (2008).
[101] B. Amadon, F. Lechermann, A. Georges, F. Jollet, T. O. Wehling, and A. I. Lichtenstein, Phys. Rev. B **77**, 205112 (2008).
[102] M. Karolak, T. O. Wehling, F. Lechermann, and A. I. Lichtenstein, J. Phys.: Condens. Matter **23**, 085601 (2011).
[103] K. Byczuk, M. Kollar, K. Held, Y. F. Yang, I. A. Nekrasov, T. Pruschke, and D. Vollhardt, Nat. Phys. **3**, 168 (2007).
[104] R. Eguchi, A. Chainani, M. Taguchi, M. Matsunami, Y. Ishida, K. Horiba, Y. Senba, H. Ohashi, and S. Shin, Phys. Rev. B **79**, 115122 (2009).
[105] X. Deng, M. Ferrero, J. Mravlje, M. Aichhorn, and A. Georges, Phys. Rev. B **85**, 125137 (2012).
[106] X. Y. Deng, L. Wang, X. Dai, and Z. Fang, Phys. Rev. B **79**, 075114 (2009).
[107] R. J. O. Mossanek, M. Abbate, and A. Fujimori, Phys. Rev. B **74**, 155127 (2006).
[108] R. J. O. Mossanek, M. Abbate, T. Yoshida, A. Fujimori, Y. Yoshida, N. Shirakawa, H. Eisaki, S. Kohno, P. T. Fonseca, and F. C. Vicentin, Phys. Rev. B **79**, 033104 (2009).
[109] R. J. O. Mossanek, M. Abbate, T. Yoshida, A. Fujimori, Y. Yoshida, N. Shirakawa, H. Eisaki, S. Kohno, and F. C. Vicentin, Phys. Rev. B **78**, 075103 (2008).
[110] H. Wadati, A. Chikamatsu, M. Takizawa, H. Kumigashira, T. Yoshida, T. Mizokawa, A. Fujimori, M. Oshima, and N. Hamada, J. Phys. Soc. Jpn. **78**, 094709 (2009).
[111] F. Aryasetiawan, K. Karlsson, O. Jepsen, and U. Schönberger, Phys. Rev. B **74**, 125106 (2006).
[112] T. Miyake and F. Aryasetiawan, Phys. Rev. B **77**, 085122 (2008).
[113] L. Huang and Y. Wang, Europhys. Lett. **99**, 67003 (2012).
[114] K. van Benthem, C. Elsässer, and R. H. French, J. Appl. Phys. **90**, 6156 (2001).
[115] M. Gatti and M. Guzzo, Phys. Rev. B **87**, 155147 (2013).
[116] S. Kohiki, M. Arai, H. Yoshikawa, S. Fukushima, M. Oku, and Y. Waseda, Phys. Rev. B **62**, 7964 (2000).

[117] Y. Nomura, M. Kaltak, K. Nakamura, C. Taranto, S. Sakai, A. Toschi, R. Arita, K. Held, G. Kresse, and M. Imada, Phys. Rev. B **86**, 085117 (2012).
[118] N. E. Zein, S. Y. Savrasov, and G. Kotliar, Phys. Rev. Lett. **96**, 226403 (2006).
[119] K. Held, R. Peters, and A. Toschi, Phys. Rev. Lett. **110**, 246402 (2013).
[120] S. Ismail-Beigi, arXiv:1406.0772 [cond-mat.mtrl-sci]
[121] A. van Roekeghem, T. Ayral, J. M. Tomczak, M. Casula, N. Xu, H. Ding, M. Ferrero, O. Parcollet, H. Jiang, and S. Biermann, arXiv:1408.3136 [cond-mat.str-el].
[122] R. Sakuma, P. Werner, and F. Aryasetiawan, Phys. Rev. B **88**, 235110 (2013).
[123] T. Kotani, M. van Schilfgaarde, and S. V. Faleev, Phys. Rev. B **76**, 165106 (2007).